FACTA UNIVERSITATIS
Series: **Electronics and Energetics** Vol. 34, Nº 3, September 2021, pp. 333-366
https://doi.org/10.2298/FUEE2103333T

Original scientific paper

A COMPREHENSIVE OVERVIEW OF RECENT DEVELOPMENTS IN RF-MEMS TECHNOLOGY-BASED HIGH-PERFORMANCE PASSIVE COMPONENTS FOR APPLICATIONS IN THE 5G AND FUTURE TELECOMMUNICATIONS SCENARIOS*

Girolamo Tagliapietra, Jacopo Iannacci

Center for Sensors and Devices (SD) Fondazione Bruno Kessler (FBK),
Trento-38123, Italy

Abstract. *The goal of this work is to provide an overview about the current development of radio-frequency microelectromechanical systems technology, with special attention towards those passive components bearing significant application potential in the currently developing 5G paradigm. Due to the required capabilities of such communication standard in terms of high data rates, extended allocated spectrum, use of massive MIMO (Multiple-Input-Multiple-Output) systems, beam steering and beam forming, the focus will be on devices like switches, phase shifters, attenuators, filters, and their packaging/integration. For each of the previous topics, several valuable contributions appeared in the last decade, underlining the improvements produced in the state of the art and the chance for RF-MEMS technology to play a prominent role in the actual implementation of the 5G infrastructure.*

Key words: *RF-MEMS, switches, packaging, phase shifters, attenuators, filters*

1. Introduction

Since the first discussion of RF-MEMS technology in late `90s, research and expectations concerning this topic have followed a fluctuating path, alternating the sensation of a general maturity and the need of some improvement to allow its practical utilization. After an initial enthusiasm towards RF passives based on MEMS, triggered by their outstanding performances, a subsequent phase of research was needed to overcome practical limits of these electro-mechanical systems, such as reliability and the possibility to package and integrate the devices with other existing technologies. Once these issues

Received March 08, 2021; received in revised form April 05, 2021
Corresponding author: Girolamo Tagliapietra
Center for Sensors and Devices (SD) Fondazione Bruno Kessler (FBK), Trento-38123, Italy
E-mail: gtagliapietra@fbk.eu
* An earlier version of this paper was presented at the 1st International Conference on Micro/Nanoelectronics Devices, Circuits and Systems (MNDCS 2021), 29 - 31 January, 2021, in Silchar, Assam, India. [1].

were addressed and RF-MEMS reached a renewed solidity, their supposed wide-scale market absorption in RF and millimeter wave communications was opposed by a scenario already dominated by cheaper and more consolidated technologies. In fact, advantages and commendable performances of RF-MEMS were not essential for the implementation of communication standards at the time [2]. Nevertheless, the last half decade portrays a more encouraging scenario: an increasing presence of RF-MEMS on the market, determined by a general maturity of this technology.

Nowadays, components based on RF-MEMS are commonly available [3], so that to be employed in base stations [4] and mobile devices [5]. Moreover, RF-MEMS are predicted to play a prominent role in the deployment of the emerging 5G mobile communication standard, capitalising on their remarkable features of reconfigurability, low power consumption and RF performances along wide portions of frequency spectra [6]. Differently from previous opportunities, in the current scenario, the increasing interest towards RF-MEMS is actually driven by the needs of market.

The use of femtocells, picocells and microcells to achieve high data rates imposes the employment of reliable, fast and wideband devices, capable to operate along frequency bands below 6 GHz and up to (24.25-29.5) GHz, (37-43.5) GHz, and (64-71) GHz bands, depending on the specific country [7][8]. From a more "macroscopic" point of view, the use of highly reconfigurable MIMO antennas, together with proper beam forming and beam steering of the basic radiation pattern is introduced to maximize the bandwidth available to users [7]. As mentioned in [9], in order to properly implement a network characterized by such variety of access points, various classes of powerful RF passives are required, including:

- Very-wideband switches and switching networks (e.g. MPMT - Multiple Pole Multiple Throw), characterized by low losses, high Isolation and extremely low cross-talk between adjacent channels along the aforementioned frequency bands.
- Reconfigurable filters with substantial rejection along stopband and minimal attenuation along the passband.
- Very-wideband impedance tuners with multiple states.
- Programmable attenuators with multiple configurations and constantly at attenuation along the considered portions of spectrum.
- Very-wideband digital/analog phase shifters with multiple achievable values of phase shift.
- Hybrid devices, comprising both attenuation and phase shifting capabilities into a single device.
- Miniaturized antennas and antenna arrays permitting monolithic integration of the radiating element with abovementioned components.

Thus, depending on the specific desired functionalities, RF-MEMS devices that could be adopted for implementation of 5G standard should satisfy different specific constraints. However, despite the variety of factors that may influence the requirements for a particular component, it is possible to quantitatively outline a set of reference performance to be pursued, which is reported in Table 1. As reported in [10][11], in the framework of MEMS devices, this set of reference performance must be matched with the separate and underlying issue of reliability.

The goal of the present work is to provide a general overview about the state of the art of some RF-MEMS devices, which are considered as key components of RF front ends in the abovementioned 5G scenario. Switches are taken into account in Section 2 as one of the first components to be implemented by this technology, and for their massive presence in almost every complex RF-MEMS and non-RF-MEMS device. The section is complemented by a set of common guidelines for an optimal design of RF-MEMS switches. Packaging is considered in Section 3 as a critical step to enhance reliability, and to guarantee the practical integration of such devices on common platforms. Since beam forming techniques are basically performed by attenuating and phase-shifting the signal feeding a radiating element, phase shifters are discussed in Section 4, including their most common architectures. For the same reason, attenuators are treated in Section 5. As critical components in every RF front end, filters are treated in Section 6. These different topics are presented by explaining their basic working principles, and examining several research contributions available in the scientific literature.

Table 1 Desirable characteristic features for devices operating in 5G network.

Feature	Desired Value	Motivation
Frequency range	<6 & (24.25-71) GHz	The diversification of the infrastructure imposes such wide range. Mobile terminals will have to operate correctly when connected to base stations or cells.
Isolation	> -30 or -40 dB	A crucial feature in reconfigurable switch- based passives, it should be as high as possible.
Loss	< -1 dB	Given the multiple components housed in common RF front ends, single losses should be minimized along the widest achievable frequency span.
Cross-talk	< -50 or -60 dB	Presence of MIMO systems and closely spaced components prescribes maximum isolation between adjacent channels.
Switching time	< 200 or 300 µs	The low latency required by the diversified network requires fast commutation of switching devices.
Control voltage	< 2 V	Compliance with typical bias voltages of circuits and avoidance of *ad hoc* additional circuitry in mobile devices.

2. Switches

RF-MEMS based switches represent one of the early and principal components in this field of research. They have been investigated since the second half of 1990s and they are part of almost all complex networks and devices implemented in such a technology.

In order to play a prominent role in the current 5G paradigm, switches have to comply with the specific requirements reported in Table 1, together with a satisfying reliability, which should be greater than one billion cycles in some applications. Many valuable research solutions addressed the above-mentioned requirements in the last years, although trade-offs are generally needed between electrical and mechanical performances.

From the point of view of classification, the movable membrane allowing or avoiding the electrical connection of the signal line to the output port, or to RF ground, may realize a ohmic (metal-metal) or capacitive (metal-dielectric) contact; on the basis of the contact, the switch will be ohmic or capacitive. The target of the connection (signal line or ground) determines the series or shunt nature of the device; hybrid series-shunt implementations are also achievable by particular arrangements [12]. The membrane may move vertically or horizontally, while its structure may be based on a cantilever or a clamped-clamped type, employing different shapes of beams and membranes. Actuation may take place by piezoelectric, electrothermal, electromagnetic or electrostatic transduction mechanism, with the last one being the most widely employed.

From a practical point of view, Isolation performances of ohmic switches are quite broadband, limited only by the capacitance between the movable membrane and the signal line, when the membrane is not actuated. This capacitance determines a decreased impedance as frequency increases, affecting overall isolation of the device. In case of capacitive switches, the contact point is covered by a dielectric layer. This determines a low capacitance in non-actuation "OFF" state, and a high capacitance when the membrane is actuated in "ON" state. Since this limits the Isolation performances at both high and low frequencies, capacitive switches can be considered more narrow-band. Due to this dynamics of their capacitance values, capacitive switches are usually evaluated on the basis of their "ON/OFF" capacitance ratio, which should be as high as possible. Additional details concerning advantages or vulnerabilities of such devices in terms of structure, performances, frequency range of usability are investigated in depth in [11].

Considering the large amount of literature in this field, some interesting proposals of the last half decade are considered. To this end, Table 2 is provided for a better comparison of the discussed research items in terms of their characteristic parameters.

2.1. Ohmic Switches

Considering ohmic switches, [13] presents a buckle-beam structure, whose actuation follows a vertical movement to connect the two interrupted sections of the signal line, thanks to a buried electrode. The beam structure is based on a Chevron thermal actuator, in which the provided voltage causes heating and deformation of the structure, with consequent horizontal displacement and de-actuation. Its working principle is represented in Figure 1a. Besides its remarkable electrical performances within the measured (0-20) GHz range, the device based on silicon substrate has been thermally characterized in the range from -20 to 140°C to test possible detrimental effects of common packaging processes on the original structure. The results demonstrate minimal variations of pull-in (actuation) voltage and losses.

With the target of a device operating at D band ((110-170) GHz), [14] proposes an SPDT (Single Pole Double Throw) switch integrated in BiCMOS (Bipolar CMOS) technology, based on an initial T-junction connected to two terminal SPST (Single Pole Single Throw) switches. Each SPST switch is encompassed in a cavity containing two actuation electrodes on both sides of elevated signal line, an overhead membrane, and a metallic plate for protection on top of the cavity, as reported in Figure 1b. The actuation of the membrane will connect the signal line to ground, isolating the corresponding output port. By choosing an actuation voltage of 60 V, the authors reached switch-on and switch-off time smaller than 10 μs.

Another substantial contribution comes from [15], in which the traditional series ohmic cantilever switch is provided with two additional cantilevers allowing a shunt connection to ground of the CPW (Coplanar WaveGuide), as shown in Figure 1c. Actuation of additional shunt connections has a dual purpose: decreasing the voltage swing on the main series contact and increasing Isolation of the output port. This protection mechanism has proven to extend reliability of this 400x300 μm_2 device up to 500 million cycles with 1 W RF power.

Beside electrical performances, the switching time is remarkable too, being 30.4 μs and 39.8 μs for switch-on and switch-off time, respectively.

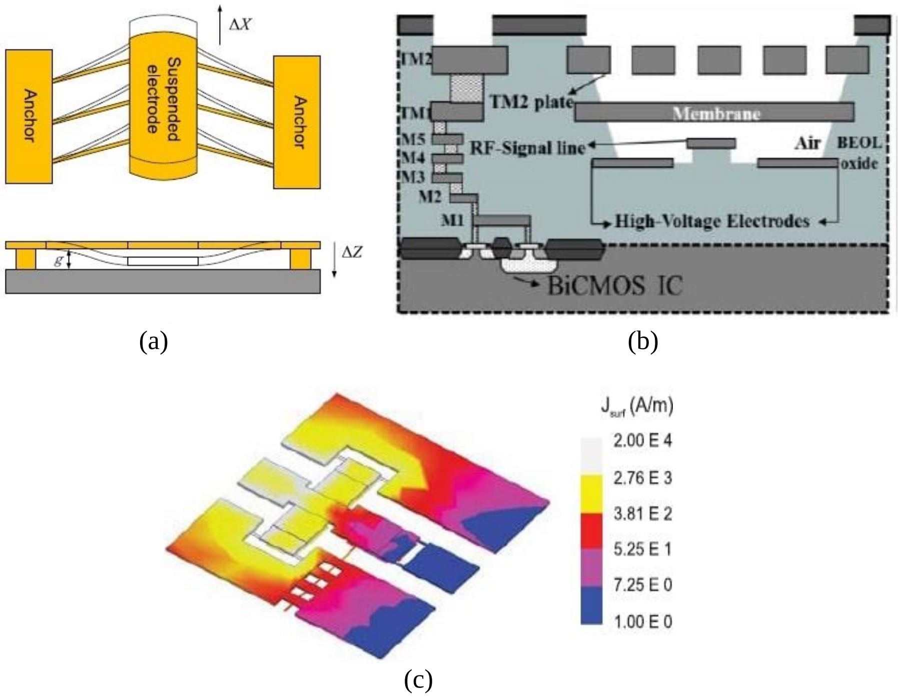

Fig. 1 (a) Movable membrane reported in [13], (b) cross section of switch cavity reported in [14], (c) surface current distribution on switch realized in [15] when lateral cantilevers are actuated to ensure maximum isolation.

In [16] a traditional series ohmic switch based on GaAs MMIC (Monolithic Microwave Integrated Circuit on Gallium Arsenide) technology is discussed, with a series of etched holes on the surface of the membrane, in order to decrease the pull-in voltage. Power handling characterization demonstrated acceptable performances up to 36 dBm, while reliability of $2.4x10^7$ cycles has been verified.

A more innovative design is reported in [17], where a laterally moving switch is proposed in order to connect the two terminations of the signal line. The movable section is always in touch with the input sections, and it comes in touch with the output section by electrostatic actuation. Triangular beams in the central part of the membrane structure provide mechanical restoring force, to move the section back to its rest position. A voltage of 90 V must be applied to ensure proper contact between the signal lines, with a 38 and 57 μs for switch-on and switch-off time, respectively. Performances for an application in 5G scenario has been considered at 3.5 GHz and 28 GHz. More complex networks have been implemented by this basic switch, including SPDT, SP3T (Single Pole 3 Throws), and SP6T (Single Pole 6 Throws), showing to be operational beyond 1 billion cycles with 1 W RF power. Footprint of these devices based on alumina substrate does not exceed 0.7 mm_2.

Another design has been simulated in [18], comprising: a cantilever vertical switch, with serpentine shaped beams, a center membrane and two free ends (contacts) provided with holes. The presence of holes on membrane and free ends, a 2.4 μm air gap, the choice of material and serpentine shaped beams allowed authors to reach a simulated low actuation voltage and commendable switch-on time of 55 μs. Moreover, the presence of two contact points is intended to increase both reliability and current-carrying capabilities of the device, decreasing the occurrence of detrimental surface nonidealities on the entire contact area.

2.2. Capacitive Switches

Considering capacitive switches, significant contributions have been proposed by [19][20][21], covering different aspects. The first one concerns a 4-beams cantilever structure: each beam is placed on a corner of a square area, each one provided with its shared tether and two springs. Stability of the structure against stress gradient is guaranteed by a central joint. Underlying dimples are employed to prevent a collapse of the structure and instability of capacitance value. Fabricated on quartz substrate, this 400x400 μm_2 device has a switch-on time of 55 μs. Besides the original design, depicted in Figure 2a, such work is remarkable in terms of power handling capabilities: the device has been characterized in its pull-in and de-actuation voltage, showing acceptable variations within (1-12) W. Hot switching conditions are also evaluated, demonstrating little sensitivity of the capacitance to temperature variations within 25-125°C.

Focused on Ka-band, and on a design minimally affected by hard fabrication temperatures, [20] proposes a folded-leg structure characterized after packaging process. Both actuation voltage and up-state capacitance exhibited minimal changes after 200°C thermal treatment, demonstrating a stable behavior of such quartz-based device during the fabrication process.

Equally focusing on Ka-band, [21] offers a device provided with an actuation electrode on both sides of signal line. Vertical movable membrane actuates in just 15 μs, and it features large perforated areas between surfaces devoted to actuation and capacitive coupling, connected to CPW ground by meandered beams. As indicated by Table 2, measured electrical parameters are remarkable, and this is also due to the high capacitance ratio of this roughly 1 mm_2 device, fabricated on high resistivity silicon.

The implementation proposed in [24] is marked by remarkable performances as well, since it exhibits minimal Insertion Loss along a wide frequency range, with a reduced actuation voltage (3.5 V). In fact, when all its membranes are actuated, an Insertion Loss smaller than 0.1 dB is achievable in the (0-25) GHz range. The simulated 640x820 μm_2 structure is based on silicon substrate and it is embodied in a CPW configuration with four cantilever membranes, each one provided with a single serpentine shaped beam. Activation of a single or multiple membrane determines different configurations, in which Return Loss is smaller than -20 dB along intervals varying from 1.6 to 16.1 GHz.

Targeting K-band satellite applications, [22] introduces a simple and effective design on silicon nitride, simultaneously achieving low actuation voltage (4.7 V) and Insertion Loss (- 0.3 dB) up to 45 GHz. Capitalising on meandered beams, a traditional rectangular perforated membrane with stepped profile, and 1.7 μm air gap, a structure with 175 μs switch-on time and high capacitance ratio (132) is obtained.

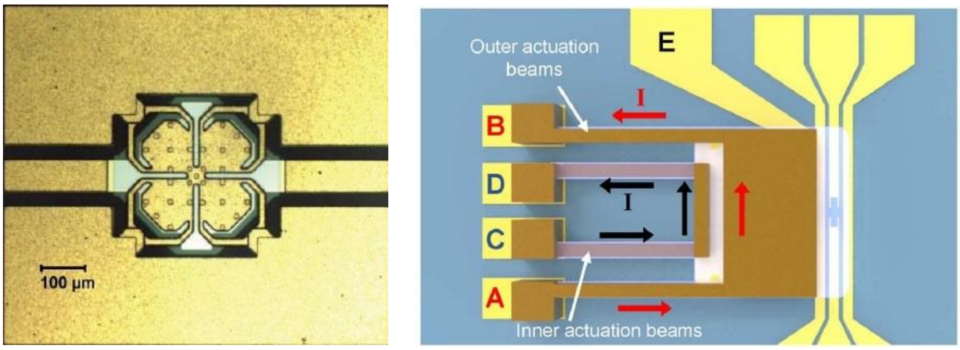

(a) (b)

Fig. 2 (a) Top view of the concept described in [19], (b) Conceptual representation of capacitive switch realized in [23].

A more complex device is suggested by [23], combining thermal actuation and electrostatic holding: the first for the actual downward or upward movement, and the second for holding the actuated membrane. In this way, low actuation voltage is achieved, still involving low power consumption. As visible in Figure 2c, the moving membrane is composed by two metal layers: the first one for upward (C and D electrodes) and the second for downward actuation (A and B electrodes), with an interposed dielectric layer. The holding electrode (E) completes the device, attracting the first layer and keeping the whole membrane actuated. This double electrothermal mechanism is employed also in case of stiction, in order to provide additional restoring force when the membrane is stuck because of micro-welding or charges trapped in the dielectric. In fact, its measured electrical properties remained constant up to 21 million cycles, while no stiction took place even after 80 million cycles. With an actuation and holding voltage of 0.3 and 15.4 V, this 160x300 μm_2 device demonstrates high Isolation up to 20 GHz.

Table 2 Comparison between the different discussed realizations, including ohmic and capacitive switches. Reported values of Return Loss (S11), Insertion Loss (S12 when CLOSE), or Isolation (S12 when OPEN) refer to worst value along the measured interval.

Work	Type	Measured @(GHz)	Ret. Loss (dB)	Ins. Loss (dB)	Isolation (dB)	Actuation (V)
[13]	Ohm	0-20	25	0.45	20	90
[14]	Ohm	140	-	1.42	54.5	60
[15]	Ohm	0-40	-	0.48	36	60
[16]	Ohm	1-40	20.09	0.25	22.5	17.5
[17]	Ohm	3.5&28	21&11.4	0.28&2.82	28	90
[18]	Ohm	1-40	15	0.6	19	3.1
[19]	Cap	20	8	1.1	12	55
[20]	Cap	35	18	0.3	35	25
[21]	Cap	35	27	0.29	20.5	18.3
[24]	Cap	5	28	2	49	3.5
[22]	Cap	27	13	0.3	35	4.7
[23]	Cap	2.4	-	0.28	31	15.4

2.3. Set of Reference Guidelines in Design and Optimization of Multiphysics Design of RF-MEMS

All the previously mentioned realizations exhibit respectable performances, covering different portions on the spectrum allocated to the current 5G paradigm. Bearing in mind the target requirements, some of the mentioned solutions are more favorable in terms of electrical performances, while others may be more convenient for their reliability, and others, again, for the possibility to be easily integrated with other circuits. Further solutions, instead, score viable trade-offs between all the mentioned characteristics. In any case, the existing vulnerabilities of a certain design concept can be properly addressed, depending on their nature. To this end, as pointed out in [11], there are different guidelines that may help a designer involved in the optimization of a particular device.

Starting from the electromechanical behavior of RF-MEMS, a shorter switching time can be achieved by acting on the actuation principle, as well as on the structural or electrical features of the device at stake. Piezoelectric actuation generally guarantees a faster actuation, but it is prone to unwanted parasitic actuations [25]; in particular, mismatches of lattice or thermal expansion coefficients of the different layers will determine the presence of residual stress in the structure, leading to cracks and bends [26]. From the structural point of view, multiple and large holes on the movable membranes are a wise option, since they increase the speed of actuation by reducing the damping of air. This is one of the criteria behind the design of the membrane reported in [22]. Another option consists in modulating the amplitude of the biasing waveform, as discussed in [27]. While a smaller voltage (as compared to pull-in voltage) can be adopted to maintain the membrane actuated, a short and relatively high voltage peak of voltage can accelerate the movement of the membrane.

An easier integration on common wireless or mobile devices usually requires low actuation voltages, compatible with typical supply voltages of CMOS technology (roughly from 1.5 to 6 V). Such low voltages avoid the presence of converters, saving costs and space on chips. Another beneficial effect is an enhanced reliability, provided by the reduction of mechanical shock on the movable membrane. Within the framework of electrostatic actuation, there are three main structural strategies to achieve such low voltages: decreasing the spring constant, maximizing the actuation area, and decreasing the air gap.

The spring constant of the movable structure can be lowered by adopting folded or meandered beams with reduced thickness, as in [20][22]. The negative consequence of a reduced spring constant of a structure is an attenuation of its restoring force, which, in turn, determines an increased risk of stiction (missed release of the actuated membrane after the zeroing of the actuation voltage). This issue can be counteracted by inserting additional electrodes, which could help the proper release of the membrane; but sometimes this solution is not affordable: beside the significant cost in terms of complexity of the design, in some cases, the housing of electrodes above the membrane may excessively complicate the fabrication process. In those cases, a viable option is represented by a proper exploitation of packaging, as discussed in Section 3. Maximizing the actuation area consists in maximizing the overlapping area between the movable structure and the fixed electrodes; for this purpose, designers would prefer membranes with relatively large areas devoted to actuation, and large electrodes, as in [21]. The decrease of the air gap is a viable option, but it should be carefully managed in case of capacitive switches. In that case, a small gap between the non-actuated membrane and the underlying contact layer would significantly increase the OFF-state capacitance. However, the corresponding limitation in the achievable Isolation can be compensated by matching circuits that mitigate the parasitic capacitance [28][29].

Better electrical performances of switching devices can be obtained by a wise selection of the structure and materials, or by introducing additional electrical components. In particular, structural modifications may involve the deployment of additional shunt membranes on a common series ohmic SPST switch. This choice is the one adopted in [15], demonstrating beneficial effects on Isolation. Another strategy regarding series ohmic switches is reported in [30], in which a triangular cantilever membrane acts as a tapered section of the transmission line, reducing the Return Loss of the device. In case of capacitive switches, the achievable Isolation in mainly limited by the up-state capacitance, while Insertion Loss is bounded by down-state capacitance [31]. For this reason, a common practice is to maximize the capacitance ratio. The ratio can be maximized at structural level by adopting bending structures or by introducing floating metal layers. Bending structures, such as warped beams or plates, represent a viable option, but they may lead to an increased actuation voltage. The addition of a floating layer generally represents a better solution: the metal plate on top of the upper dielectric layer does not affect the up-state capacitance, but it acts as a wider upper plate of a capacitor when the membrane is actuated. This leads to a higher down-state capacitance. The solution of a floating metal layer should be preferred also because of a practical issue: the surface roughness of the dielectric is generally not accounted in simulations. Actuated membranes with a non-uniform adhesion to the underlying dielectric layer, or surface roughness, will determine an interposed layer of air, decreasing the achievable down-state capacitance [32][33]. The adoption of the floating layer allows to overcome these practical issues.

Regarding the substrate and the dielectric, the choice of materials and their thickness is an important subject. Good electrical performances are usually obtained by using substrates with high resistivity, such as quartz, glass, high-resistivity silicon, gallium arsenide (GaAs) or silicon-on-glass (SiOG) [34][35][36]. In case of capacitive switches, dielectric materials with a high permittivity and arranged in very thin layer are preferable, since they ensure a high capacitance when the membrane is actuated. The main candidates are piezoelectric leade zirconate titanate (PZT), strontium titanate oxide ($SrTiO_3$), tantalum pentoxide (Ta_2O_5) and hafnium dioxide (HfO_2) [37][38][39]. However, while some of them are relatively expensive, the thickness of the dielectric must be chosen accordingly to the available fabrication process, and it must ensure to sustain the pull-in voltage without a breakdown.

The introduction of additional electrical components generally involves the deployment of shunt inductors or sections of transmission lines. In fact, the beams supporting the movable structure introduce some parasitic inductance, affecting the Isolation of the device. This inductance is generally compensated by introducing matching sections or reactive components [29].

Reliability is an important issue, investigated in depth in the framework of RF-MEMS devices, thus different strategies have been proposed so far. The occurrence of stiction can be mitigated or counteracted by some of the already mentioned strategies, such as the insertion of additional electrodes to enforce the release, the decrease of pull-in voltage, the modification of voltage actuation waveform or the adoption of additional shunt membranes. Beside these techniques, other expedients regarding the structure and employed materials can be listed. From a structural point of view, the most common are the use of frames with reinforcing bars on the movable structure, and stopping pillars or thin posts under the membrane [40]. The underlying idea is to prevent deformations of the membrane and its complete adhesion to the dielectric layer, in which residual trapped charges may be present. Other possibilities to overcome the problem of trapped charge is the adoption of lateral actuation mechanisms, as in [17], or the more "radical" option of a dielectric-less design [41].

An increased lifetime of the device can be achieved also by a proper selection of materials. In case of ohmic switches, stiction is mainly caused by increase of resistance, welding, fusion or transfer of metal contacts. This is generally prevented by the adoption of harder metals, such as molybdenum (Mo), palladium (Pd), tungsten (W) and rhodium (Re), often organized in multilayers [42][43][44]. In case of capacitive switches, besides charge injection and trapping, reliability is threatened by mechanical shock and the breakdown of the dielectric layer. These problems can be mitigated by using layers that may rapidly release charges, such as aluminium nitride (AlN) and PZT [45], by removing surface roughness and nonidealities, or by adopting robust structures with double dielectric layers.

3. PACKAGING

When talking about reliability of MEMS components, it is not possible to omit the closely related field of packaging. Besides enclosing MEMS structures in a "sealed" space, less sensitive to changes of temperature or humidity, packaging avoids contamination with harmful agents and external mechanical shocks. However, this indispensable interface to outer world introduces: additional costs of production, increased volume and impairment on performances of the original (naked) MEMS device. The two main choices for packaging at technology level are chip-scale and wafer-level package. The latter is the most widely employed for its lower cost, efficiency in packaging process, reduced size and decreased impairment of performances. Such a technique can rely on two fundamental approaches: application of a cap and thin-film packaging.

The former approach adopts silicon-based materials as a cap covering the device, as depicted in Figure 3a. Typical materials for the realization of the cap are represented by Benzocyclobutene (BCB), co-fired ceramic (LTCC), silicon (Si), and quartz (SiO_2). Depending on the presence (or absence) of a sealing material, interposed between the cap and the device wafer, intermediate bonding (or direct bonding) techniques are employed to seal the cap. Intermediate bonding is generally more convenient because of its relatively low temperatures ((200-400)°C), since direct bonding techniques may require up to 1000°C (in case of fusion bonding, as reported in [46]). The cap is placed on MEMS device by optical alignment and typically sealed by gold (Au), SiO_2, BCB, or SU-8.

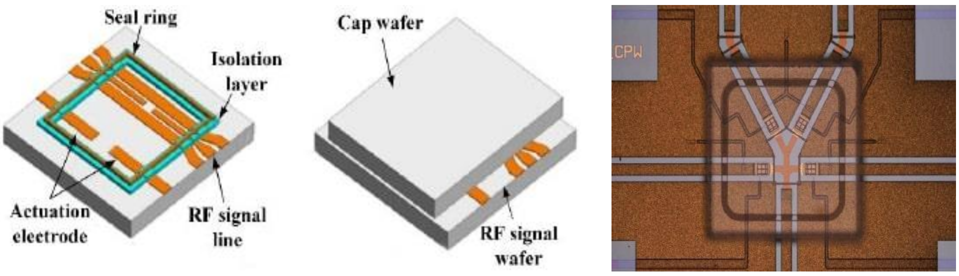

(a) (b)

Fig. 3 (a) General practical implementation of capping reported in [47], (b) detail of quartz capped SP4T (Single Pole 4 Throw) switch, reported in [48].

Examples are reported in [48][49][50][51] showing switches encapsulated by intermediate bonding techniques at temperatures in the range (200-250)°C, which have not been particularly impaired by packaging procedures. In particular [48] presents various devices, including the SP4T switch represented in Figure 3b, protected by a quartz cap fixed on substrate by epoxy polymer SU-8. Depending on the substrate flatness, two fabrication methods are proposed: one for substrates with cavities and holes, and one for flat substrates. Experimental results of electrical parameters show minimal degradation of Insertion Loss (an increase of 0.1-0.2 dB) up to 30 GHz, providing a capped device not exceeding -0.7 dB up to 40 GHz. Return Loss is slightly impaired by the impedance mismatch introduced by the cap, reaching values up to 10 dB in the range up to 20 GHz. In the remaining portion of the measured spectrum, the Return Loss of the capped device complies with the one of uncapped version along the measured range. Encapsulation did not drastically affect electro-mechanical properties. While for a shunt capacitive switch there was no change in capacitance and actuation voltage was just slightly increased, a measured SP4T switch showed a minimal change in series resistance and a decrease of actuation voltage.

A more recent contribution comes from [52], in which a silicon cap bonded by spin-coated BCB is accurately modeled and added to different switch devices. The different mounted caps have been tested in terms of resistance to shear stress, by applying horizontal force only to the cap while keeping the wafer fixed. Packages exhibited a high average break force (force needed to detach the cap) of 21 N. The increase of Insertion Loss due to the proposed package is around 0.2 dB, with an average increase of actuation voltage of 4.2 V among the nine measured switches. All capped switches show remarkably low Insertion Loss (<-0.44 dB), and reasonable Return Loss (<-20.9 dB) all over the 40 GHz measured interval, operating for more than 10.2 billion cycles.

The approach of thin film packaging generally involves a sacrificial layer placed on movable parts of a MEMS device, covered with a thin film layer. Such layer will be perforated to remove the sacrificial layer, and then covered with a proper layer for final sealing, as shown in Figure 4a. In this case, gold [53] and silicon-based materials are commonly employed solutions for the thin film, as observed in [47]. Such materials, besides various polymers, can be adopted also as sealing layer, generally patterned by deposition, evaporation and electroplating, spin-coating or plasma-enhanced chemical vapor deposition (PECVD). Examples of such technology are reported in [53][54][55][56], showing encapsulated devices still maintaining remarkable RF performances after the packaging process.

A more recent proposal comes from [57], in which a protective dielectric shell comprises an electrode, biased to ensure maximum vertical upward displacement of the movable membrane of a capacitive switch. This is beneficial both for the capacitance ratio and reliability aspects. Possible configurations of this device are represented in Figure 4b. Contact holes and release channels are etched on sides of the shell to remove the sacrificial layer; a Si_3N_4 layer is then deposited by PECVD to hermetically seal the structure. Measurements over hours of operations with square bipolar biasing voltages show that both actuation voltage and capacitance suffer from minimal variations, leading to an increase of just 0.2 dB in Insertion Loss.

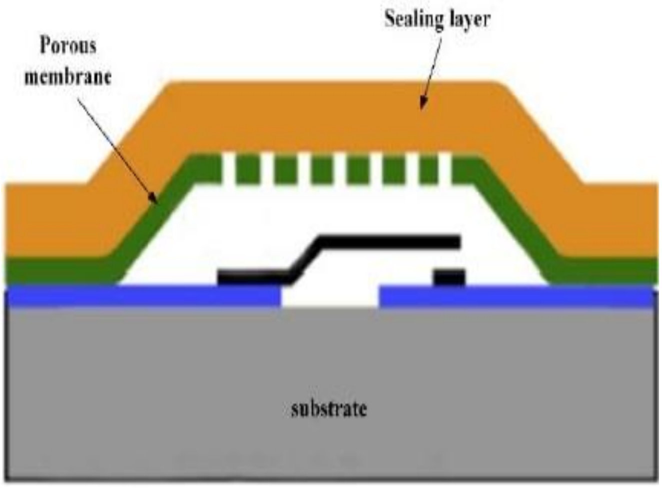

(a)

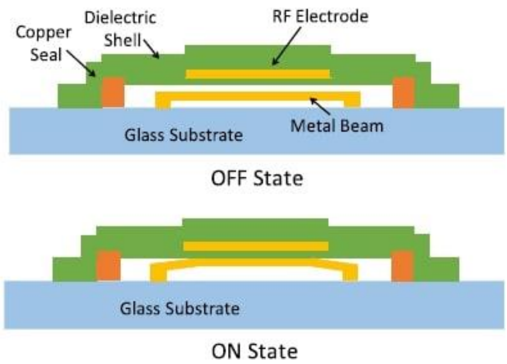

(b)

Fig. 4 (a) General practical implementation of thin-film packaging reported in [47], (b) cross section of the device reported in [57] in both its states.

An interesting contribution is represented by [58], in which an investigation regarding the amount of perforated area on the thin film for the proper release of encapsulated devices is reported. In this work, thin film layer is perforated with holes of different diameters (7 and 8 μm), and different realizations of perforated films are obtained, each one with a different percentage of perforated area. After the identification of the most appropriate percentage (at least 57%), different combinations of power and time are considered for the proper release of the considered devices. Complete 3D FEM (Finite Element Method) models of the considered realizations on gold CPW have been implemented and simulated, showing no significant variations of Return or Insertion Loss introduced by the packaging phase.

Table 3 Comparison between the different discussed packaging implementations, including both cap and thin film solutions. The provided dimensions in the order of mm, and tens or hundreds of μm, refer to dimensions of the whole packaged device.

Work	Type	Cap or Film/ sealing Materials	Dimensions (μm)	Ins. Loss (dB/@GHz)	Isolation (dB/@GHz)	Temp. °C
[49]	Cap	LTCC/Au	1.4x0.9x0.8	0.5/5	20/5	250
[50]	Cap	BCB/BCB	$2mm_2$x28	0.7/30	18/30	250
[51]	Cap	Si	5000x4000x950	0.5/6	24/2.5	-
[48]	Cap	SiO_2/SU-8	-	0.7/30	-	200
[52]	Cap	Si/BCB	-	0.4/35	35/35	250
[53]	Film	Au/SiO_2	-	-	27/2	<120
[54]	Film	Si_3N_4/Au	75x80x 1.2	-	30/2	-
[56]	Film	Na/SiO_2	- x - x4	0.45/142	51.6/142	200
[55]	Film	SiO_2/ ALX2010	<600x600x -	0.25/12	35/12	-
[57]	Film	Si_3N_4	70x50x -	2/25	8/25	-

4. Phase Shifters

Being vital components in the architecture of Phased Arrays and RF front ends, phase shifters are abundantly employed in radar systems (L, S, C, X bands), as well as for mobile and satellite communications (Ku, K, Ka bands). Current developments in terms of mobile communications, with the adoption of millimeter wave frequencies, determined an accentuated interest towards MEMS-based phase shifters. Consequently, the literature regarding this field is quite populated.

The first implementations of phase shifters based on RF-MEMS were proposed in late `90s, both concerning digital [59] and analog [60][61] realizations. Shortly after, the main topologies concerning the architecture of the proposed phase shifters were defined, according to the following classification: switched-line (SL), loaded-line (LL), distributed MEMS transmission line (DMTL), and reflection-type (RT) phase shifters.

As reported by more comprehensive books and overviews, such as [62][63][64], the working principle of switched-line devices is the switching between signal paths of different electrical length, in order to achieve the desired phase delay. However, when a wide phase shifting range or multiple small phase steps are required, such strategy may lead to bulky arrangements. Conceptually similar, the basic idea of loaded-line phase shifters is to load a transmission line with two reactive impedance networks. Often realized with stubs, capacitive or inductive loads will cause phase lags or leads respectively, while the transmission line section will ensure impedance matching. As in the case of switched-line devices, extended shifting performances will lead to bulky phase shifters.

In case of DMTL, the transmission line of the signal path is periodically loaded with varactors, changing the distributed capacitance of the line and, in turn, the line phase constant and, finally, the resulting phase delay at the output port. When wide shifting or precision performances are required, the presence of multiple MEMS capacitive membranes determines arrangements with pronounced area, high aspect ratio and prone to reliability issues.

RT phase shifters typically employ quadrature couplers with equal and tunable reflective loads connected to coupled ports, controlling the phase delay of the reflected signal. Although this approach may seem less troublesome, it is characterized by underlying trade-off between the achievable shift range and the Insertion Loss. Such trade-off is due to the need of effective modeling, design and matching of the coupler and of the reflective load.

As highlighted in [65], although phase shifters based on RF-MEMS represented a powerful solution to simplify the architecture of phased arrays, some substantial improvements were mandatory at that time. The main requirement was a general reduction of the physical footprint. Other concerns were mostly related to the employed switching units within the phase shifters, the most relevant ones being limited reliability, high switching time and limited power handling capabilities. These factors confined early RF-MEMS phase shifters to arrays with relatively slow scanning and radiated power, while the physical size prevented the integration in case low microwave frequencies were at stake (<20 GHz).

Many research solutions of the last decade remarkably faced the challenge of increasing the shifting range and phase precision, and considerable steps ahead have been made in the direction of miniaturization, still lowering insertion loss. Tables 4 and 5 are provided along the present section for a better comparison of the discussed research items in terms of their characteristics.

4.1. Switched-Line

Concerning switched-line topologies of RF-MEMS phase shifters, some relevant contributions are reported in [66][67][68]. In particular, the device presented in [66] and shown in Figure 5a has a wide shifting range and remarkable power handling capabilities (5 W), at the expense of losses (-3.1 dB Insertion Loss) and footprint (7.5x6 mm_2). The employed SP2T and SP4T switches demonstrated very limited switching time (5 μs) and high reliability (100 M cycles), despite a rather high actuation voltage of 90 V. Since both [67][68] propose 1-bit 180° phase shifters, their intrinsic simplicity allows more appreciable losses and area (9 and 15 mm_2).

Additional suggestions are offered by [69][70][71][72]. In particular, [69] suggests a 4-bit phase shifter for LTE base station, fabricated on common PCB substrate. The path from the input to the output port is composed by two sections, each one provided with four paths of different electric length, as depicted in the block scheme of Figure 5b. The switching is performed by two SPDT on both sides of a section, actuated by 90 V signal in 10 μs.

A 5-bit architecture focused on Ku band is described in [70]. As reported in Figure 5c, out of the three sections in which the device is divided, two are characterized by four paths with different electrical length selected by a SP4T switch on each side. The remaining section contains just two paths, selected by a couple of SP2T switches. By applying 53 V pull-in voltage, switch-on time is 28 μs for both kinds of micro-relays. The overall area of the device is 3.19x5.17 mm_2. In case of both cold and hot switching conditions, the device has been demonstrated with more than 10 million cycles from 0.1 to 1 W of RF power.

The 3-bit device reported in [71] has been characterized in the Ka band, and it is composed by two SP8T switches selecting one output of the available eight signal paths. With a total area of 5.9 mm_2, this phase shifter based on Alumina substrate employs switches with actuation at 65 V. Reliability measurements at room temperature reported a satisfactory behavior beyond 100 million cycles for the range of power (0.1-1) W, and beyond 30 million cycles for 2 W of RF power. Possible improvements for the two previous works are reported in [72], together with a DMTL solution for a K band phase shifter by the same authors.

Another recent proposal is provided by [73], with two realizations of 4-bit phase shifters for K and Ka frequency bands, in both cases composed by 4 sections comprising a reference and a shifting path. A couple of monolithically integrated MEMS SPST switches control the activation of each path by 45 V signal, allowing 16 phase states. Fabricated variants for K band show a footprint of 10.5x7.5 mm$_2$.

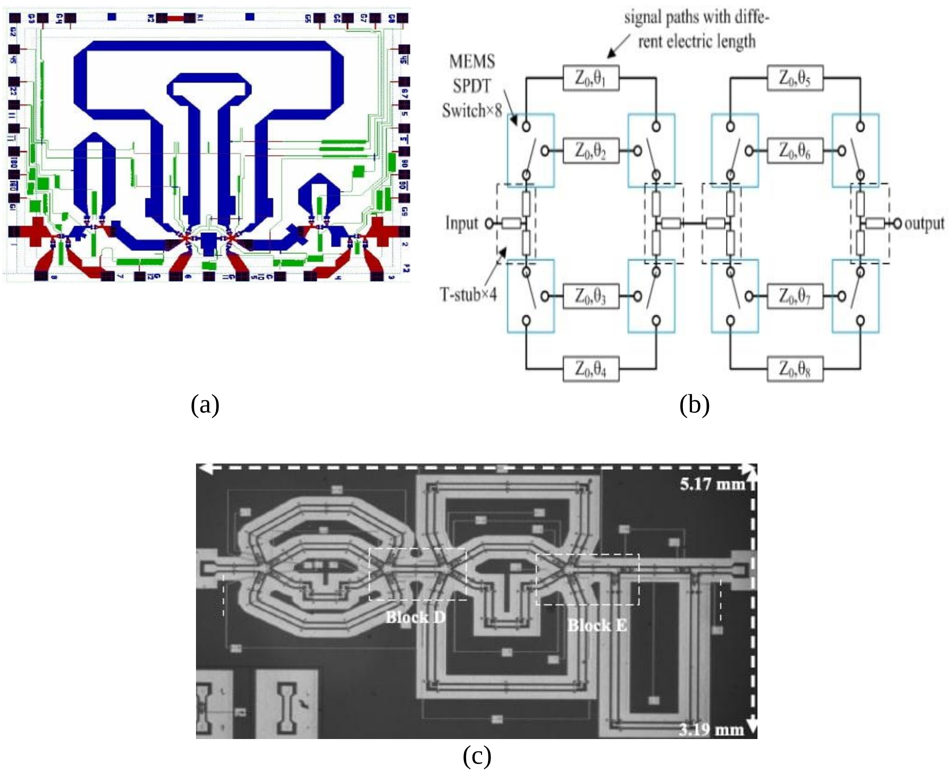

Fig. 5 (a) Switched-line phase shifter described in [66], (b) block scheme of the device reported in [69], (c) top view of architecture proposed in [70].

4.2. Loaded-Line

Regarding loaded-line architecture, noteworthy results are obtained in [74][75]. The first one describes a device composed by a transmission line periodically loaded by a total number of eight 4-bit tunable capacitive loads. The control of capacitors is achieved by (lateral) electrostatic and (vertical) electrothermal actuation. The overall 16 states allow to tune digital capacitors from 15.5 to 111.6 fF, changing phase velocity of the line and determining a maximum phase shift of 337.5°. While electrostatic actuation requires 20 V, its electrothermal requirement is just 4.8 V. The proposed phase shifter has been designed to be monolithically integrated with conventional CMOS, and involves an overall footprint of 4.32x0.5 mm_2, although the aspect ratio is still relatively high.

Another digital phase shifter is offered by [75], i.e. a 3-bit device allowing a total 315° of shift. In a more classic design, quarter wavelength microstrip sections are periodically loaded with different susceptances, sequentially composing 180°, 90° and 45° shifting sections, within an area of 20.5x6.5 mm_2.

Table 4 Comparison between the different discussed realizations of phase shifters, comprehending Switched-Line and Loaded-Line topologies. For each realization, the reported Return Loss, Insertion Loss, and phase Error referred to worst case among the various observed states are reported.

Work	Type	Measured @(GHz)	Ret. Loss (dB)	Ins. Loss (dB)	Min Shift (°)	Max Shift (°)	Error (°)
[66]	SL	1	15	3.1	5.625	337.5	-
[67]	SL	30	-	1.5	0	187	7
[68]	SL	24	19.2	1.65	0	184.6	4.6
[69]	SL	2.7	13.4	0.89	5	75	2.05
[70]	SL	17	22	3.72	11.25	348.75	1.14
[71]	SL	35	14	5.07	45	315	1.78
[73]	SL	19.5	15	6.8	22.5	180	4.5
[74]	LL	32	15	3.9	45	337.5	-
[75]	LL	2.5	8.5	4	45	315	7.9

4.3. Distributed MEMS Transmission Line

Concerning DMTL topology, multiple suggestions have been provided even only in the last half decade. Different examples are reported, covering a certain variety of possible arrangements and improvements. The most classic examples of DMTL design are reported in [76][77][78].

Being a DMTL phase shifter basically composed by a transmission line loaded with MEMS bridges, the work in [77] is the study of a simple one-bit DMTL cell aimed at the improvement of a basic switched-line 1-bit phase shifter in the range 1-6 GHz. Such study reports that adding a MEMS bridge on the shifting signal path introduces an improvement of 40% and 25% as compared to initial size and losses, respectively.

Despite the traditional design, an innovative proposal is discussed in [76]. In this work, the signal line is loaded with 26 capacitive bridges, with 7 possible lengths. Since its longer bridges need lower actuation voltage (10 V) as compared to shorter bridges (40 V), each buried electrode controlling a bridge is connected to the same DC voltage pad. In this manner, a single signal will actuate all bridges characterized by the same length, determining a precise phase shift. Such design avoids the presence of multiple control pads, reducing the footprint of this 7-states device to 7x0.8 mm_2.

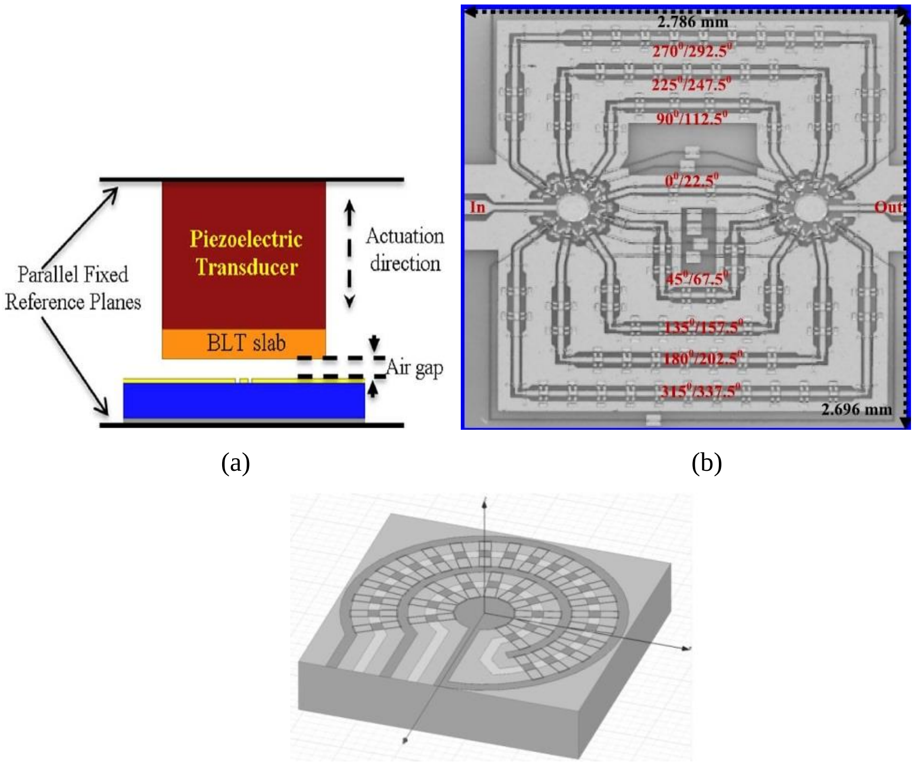

(a) (b)

(c)

Fig. 6 (a) Schematic section of DMTL phase shifter described in [83], (b) top view of 4-bit device offered by [84], (c) schematic of the arrangement proposed in [85].

Following the traditional “straight loaded line" approach, [78] emphasizes the importance of miniaturization for movable components. In particular, the fabrication of bridges with a scaled area allowed the authors to design a basic 30° delay cell with 1x0.66 mm_2 area, reduced actuation voltage (14.6 V), and low switching time (0.6 μs). Promising performances of the cell thus permitted to cascade six of them, obtaining a 180° phase shifter with 4x1 mm_2 on quartz substrate.

An improvement of the basic bridge cell loading the transmission line is provided by [79]. Besides the standard actuation electrode, two additional electrodes are introduced: each one on a side of the signal line, on a higher pillar. In this manner, besides non-actuation state, each basic cell may achieve two different capacitive states, extending its reconfigurability. By cascading 32 of such cells, the Authors propose a 6-bit phase shifter with a maximum shift of 180°, by 5.625° steps. Characterized by reasonably low actuation voltages (6.8 and 3.4 V), the device exhibits an overall length of 12.8 mm.

Additional remarkable works are represented by [80][81][82], comprising DMTL configurations working in the part of spectrum from X band to 60 GHz, with considerably small losses and phase error, investigated in depth also in terms of reliability.

A more compact and innovative design is proposed in [83], with two horizontal parallel fixed plates: the lower is the base for the dielectric of the CPW, while the upper is the support to which a piezoelectric transducer is attached. As it is shown in Figure 6a, on the lower side of the transducer, a slab with high dielectric constant is stuck. The 35 μm air gap separating the slab from the underlying CPW is varied by the transducer, inducing broad changes of load (and thus phase delay) on the signal line. In order to extend the achievable phase shift, a grating and a serpentine shaped CPW line have been investigated, besides standard straight CPW configuration. With an overall length of 3 mm, the device is fabricated on simple high-resistance silicon.

As compared to previous designs, an arrangement that permits to drastically reduce the aspect ratio of the overall device is presented in [85]. In this case, a 5-bit phase shifter is implemented by a spiral-shaped CPW configuration of the signal line and loaded with 31 capacitive MEMS switches, as depicted in Figure 6c. The actuation of switches takes place by groups. In details, the switches are divided into five groups, involving shifts of 11.25°, 22.5°, 45°, 90° and 180°. The device has a remarkable footprint of 2.6x2.6 mm_2.

One last proposal to be mentioned about DMTL phase shifters is [84]. In this work, two compact devices (3 and 4-bit) are proposed, both exploiting the advantages of combining switched-line and DMTL topologies. In case of the 3-bit device, two bits control the SP4T switches (selecting one of the four delay lines), while one bit controls capacitive bridges loading the lines. The same principle applies to the 4-bit version displayed in Figure 6b. Both devices are designed to operate in Ka band, at 35 GHz, showing valuable maximum Return Loss (<-12 dB), contained phase error (<3.8°), and compact sizes of 2.24x1.91 mm_2 and 2.78x2.69 mm_2, respectively. Moreover, both devices exhibit a low aspect ratio. Devices have been evaluated also in terms of reliability, sustaining more than 1 billion cycles with 0.1 W of RF power in cold switching conditions, and more than 400 million cycles with 0.5 W in hot switching conditions (85°C). In addition, the inclusion of the two phase shifters within a low cost package has been accurately characterized.

4.4. Reflection Type

Regarding the Reflection Type architecture, research contributions in the last decade mainly focused on the improvement of both quadrature coupler and reflective loads.

Some noteworthy contributions are represented by [86][87][88]. In the first one, a 2-bit device composed by two directional couplers (3dB branch line) and four loads is presented. Activation of loads connected to the output ports of a coupler by MEMS switches determines a 45°, 180° or 225° shift. Implemented on a Sapphire substrate, the whole circuit covers an area of 7.9x4 mm_2. This device, which has been conceived for the Ka band, was characterized also in terms of power handling capabilities, showing a commendable behavior up to 32 dBm input power.

Among the different advances in the field of RF-MEMS phase shifters listed in [87], a couple of them are interesting from the point of view of the design strategy. In particular, for the design of devices working in K and Ka band, a hybrid distributed-reflective architecture is adopted. When small shift (22.5° or 45°) is required, only the input microstrip lines of the coupler are loaded with capacitive radial stubs by MEMS switches, without actuating any load on the other ports of the coupler. Differently, when a higher shift is required (from 90° to 270°), capacitive loads are activated on the output lines of the coupler by switches. Two packaged realizations of such architecture have been measured in their 16 phase states, one working at 15 GHz and shown in Figure 7a, while the other at 21 GHz. The packaged devices proved to be able to sustain over 250 billion switch actuations.

A robust implementation of a phase shifter mounted on a base station for electronically scanned antennas, is reported in [88]. It is composed by two stages: one introducing 0°, 11.25°, 22.5° or 33.75°, while the other introducing 0°, 45° or 90° shift. Each stage comprises a quadrature coupler and LC loads, both realized by microstrip. Loads are selected by commercial Omron SPDT MEMS switches. The proposed device is realized on common RO4003 substrate. The employed switches have been extensively characterized in terms of reliability: at 2 GHz RF power and hot switching conditions, switches operated beyond 100 M cycles (in (0.1-0.3) mW range) and slightly more than 5 M cycles (in the (0.5-1) W range).

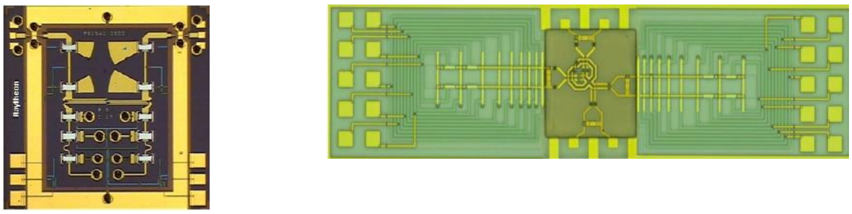

(a) (b)

Fig. 7 (a) Realization of Reflection Type phase shifter working at 15 GHz, described in [87], (b) top view of the architecture proposed by [89].

A significant suggestion in terms of reconfigurability and shifting range comes from [90]. After a detailed characterization of a proposed reconfigurable quadrature hybrid coupler based on MEMS varactors, this one is adopted in the implementation of a 360° phase shifter. In this case, each output branch of the reconfigurable coupler is connected to a dual-resonant LC load, realized by two parallel branches connected to ground, each one including an inductor and a 5-bit varactor, controllable by 35 V actuation. This kind of load allows a 360° phase shift, without the need of including another stage. By acting on the 10 bits is then possible to achieve 1024 phase states, although some of them will be quite similar for what concerns the resulting shift.

A device operating at K band, with more classic design, is proposed in [91]. A Lange coupler and two reflective paths, each one provided with three switches along the lines, are enclosed in the footprint of 2.45x1.77 mm_2. The length of short-ended lines can be decreased by actuating one of the shunt switches. While the total length of the load line corresponds to a 135° shift, actuation may introduce 90°, 45° or 0°.

The same concept is exploited in [89], where a coupler made by folded broad-side coupled lines is presented, after a detailed theoretical analysis of the qualities to be pursued in the design of both the coupler and the reflective loads. Its ultrawideband performances comprehend: reflection coefficients of all ports smaller than -25 dB and isolation greater than -28 dB, over the whole (70-86) GHz interval. Eight switches are comprised in such 3-bit device depicted in Figure 7b, for a total footprint of 2.68x0.70 mm_2, considering the device and different pads.

The most recent analog implementation is offered by [92], in which output ports of the Lange coupler are connected to a LC reflective load (three inductive line sections spaced out by couples of shunt varactors) in a CPW configuration. The capacitance of contactless varactors loading the lines is simultaneously tuned from 85 to 200 fF by the control voltage applied to the pads of a Chevron electrothermal actuator, thus determining the output phase shift of this 4x2.6 mm_2 device. The continuous tuning range covers 120° shift, achievable by 8 V control signal.

Table 5 Comparison between the different discussed realizations, comprehending Distributed MEMS Transmission Line and Reflection Type topologies. For each realization, Return Loss, Insertion Loss, and phase Error referred to the worst case among the various configurations are reported.

Work	Type	Measured @(GHz)	Ret. Loss (dB)	Ins. Loss (dB)	Min Shift (°)	Max Shift (°)	Error (°)
[76]	DMTL	30	13	1.7	-	106	-
[78]	DMTL	22	12	3	30	180	-
[79]	DMTL	30	16	0.8	5.625	180	<1
[83]	DMTL	30	12	2.55	-	170	-
[85]	DMTL	40	9.9	15.1	11.25	348.75	3.72
[84]	DMTL	35	14-12	3.8-5.4	45-22.5	315-337.5	2.3-3.8
[86]	RT	26	7	2.5	45	225	-
[87]	RT	15-21	10-12	2.2-2.2	22-22	337-337	7-5.3
[88]	RT	2	21	0.93	11.25	123.75	5
[90]	RT	2	25	2.4	-	360	11.25
[91]	RT	20	13.61	1.61	45	135	1.15
[89]	RT	74	18	4.9	22.5	195	8.6
[92]	RT	28	15	6.35	-	120	-

5. Attenuators

Differently from the previous two kinds of device, RF-MEMS based attenuators are not characterized by a dense presence of scientific literature, remaining a relatively niche scenario. Nonetheless they also represent key components in the evolution towards the IoT and 5G paradigms, together with impedance tuners, filters and resonators.

Among the remarkable characteristics typical of RF MEMS, in case of attenuators the most valuable are represented by reconfigurability, broadband behavior and good linearity. Desirable attenuators should exhibit multiple configurations of attenuation, each one with a flat and stable value of impedance along a wide range of frequencies. Table 6 is provided at the end of the present section for a better comparison of the discussed proposals in terms of their characteristic parameters.

From a general point of view, devices operating by both digital or analog control are present in the literature. Since the first decade of the new millennium, the first one is the most widespread, as it is possible to observe by looking at [93][94].

In [93] a 6-bit attenuator is presented: within the 8.77 mm_2 device encompassed in CPW configuration, two SPDT switches and two branches loaded with six series resistors and corresponding bypass cantilever membranes are comprised. While switches are meant to select one branch or another by ~15 V actuation, cantilevers will shorten or load resistors on the selected branch. With 64 possible impedance states, the device demonstrated remarkable linear performances in terms of Insertion and Return Loss. Conceptually similar, [94] proposes a CPW-based structure in which signal line crosses an initial section with 3 series resistors, and then separates into two parallel lines: each loaded with 3 resistors and their movable membrane. The two branches eventually meet to form the output line, as shown in Figure 8a. By an actuation voltage between 70 and 80 V, and by 7-bit sequences is then possible to control 128 possible impedance states. Also in this case the performances are stable, demonstrated over a wider interval.

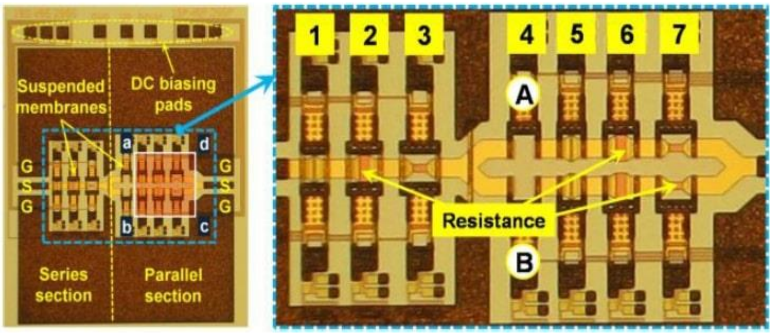

(a)

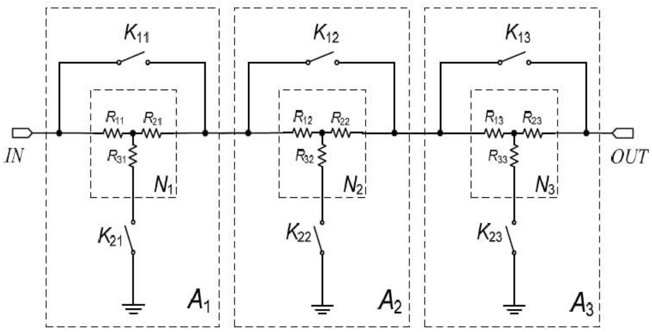

(b)

Fig. 8 (a) Complete architecture described in [94], (b) schematic of device proposed in [96].

Substantially new contributions appeared only in the last half decade with [95][96], both proposing 3-bit attenuators enclosed in CPW configuration and demonstrated up to 20 GHz.

With a reduced footprint of 3.2 mm_2, [96] offers a structure composed by three equal sub-units in series on the main signal line, determining an attenuation of 5, 10, 20 dB respectively. As depicted by the schematic of Figure 8b, each sub-unit is composed by a T-shaped resistive network and two cantilever switches: one switch rules shunt connection to ground, the other allows to bypass the two series resistive loads. The proposed design achieves 8 different states with a limited attenuation error, at the price of 70 V actuation.

In a similar way, [95] proposes a device composed by three cascaded sub-units of 10, 20, 40 dB attenuation. Each sub-unit comprises a T-junction power splitter, leading to an unloaded branch or to a branch loaded with π-shaped resistive network by its SPST switch. Specular SPST switches and T-junction complete the sub-unit. Such design allows to reach wide attenuation (70 dB), with a reduced pull-in voltage (30 V) and footprint (2.45x4.34 mm_2).

Previous research items are generally demonstrated over a limited range of frequencies, with a limited number of possible states (except [93][94]).

The first offer for an attenuator covering a wider spectrum came with [97]. In this work, a 8-bit device is presented, measured in the interval (0.01-110) GHz. Enclosed within CPW configuration and with an overall footprint of 3x1.95 mm_2, the attenuator is substantially composed by eight cascaded modules of ohmic switches along the main RF signal line, actuated by 45 V signals. Depending on the type of module, each switch will contribute to shorten (when actuated) the resistor in series on the signal line or to connect (when actuated) signal line to a shunt resistor to ground. The latter module thus may operate or avoid shunt resistive path to ground, while the former module may shorten the series resistor, and so on, alternately. Such asymmetric network is measured under a wide variety of configurations, considering VWSR (Voltage Wave Standing Ratio), Insertion and Return Loss, and identifying the most advisable configurations and causes of the unadvisable ones.

The first proposals of analog attenuators came only during the last couple of years. In [98], Authors present a design based on CPW meandered configuration. A membrane with low-resistivity silicon slab is deployed over the signal line, with a highly magnetized permanent magnet on the upper side facing an overhead planar spiral coil. The direction of the current determines the attraction (or repulsion) of the underlying magnet and membrane, while the amount of current determines the variation of the gap between the slab and the signal line and, in turn, the quantity of signal power absorbed by the silicon slab. This 2x5 mm_2 device exhibits low Insertion Loss, for an attenuation range of 16.4 dB.

A radically different design is proposed in [99]. This work is substantially based on two quadrature hybrid coupler and two varactors. While “Isolated” ports of the couplers are terminated with a matched load, the corresponding “Through” and “Coupled” ports of couplers are connected by separate RF lines, each loaded with a shunt varactor. The plates of a varactor are on the two sides of the RF line and are moved by an electrothermal Chevron-type actuator, driven by a control signal with maximum value of 9.8 V. Beside actuation voltage, the area of the device is moderate (3.8x3.1 mm_2), as well. Despite the limited attenuation and frequency range, the previous two proposals represent remarkable steps ahead in the direction of further low-cost and low-power reliable RF-MEMS attenuators.

Table 6 Comparison between the different discussed realizations of attenuators**.**

Work	Range (GHz)	Measured @(GHz)	Ret. Loss (dB)	Ins. Loss (dB)	Max Att. (dB)	Step (dB)	Error (dB)
[93]	0.05-13	8	15	1.8	19.7	-	-
[94]	0.1-40	20	-	2.5	38.5	-	-
[95]	0.1-20	0.1-20	11.9	0.73	70	10	<3%
[96]	0-20	0-20	12	2	35	5	<5%
[97]	0.01-110	20	-	5	45	-	-
[98]	21.5-26.5	23.5	18	1.2	17.6	-	<0.2%
[99]	58-62	60	20	10	25	-	-

6. FILTERS

Filters play a crucial role in every RF front-end, enabling a suitable signal-to-noise ratio for the desired signal contributions and rejecting the out-of-band noise within the desired frequency bands. Moreover, by considering the growing overpopulation of the limited available spectrum in recent years, it is possible to understand why the role has gained an increasing relevance [100]. Given the additional portions of spectrum provided by 5G paradigm and the required compliance with different communication standards, the presence of agile reconfigurable filters represents a stringent need for radio front-ends of future mobile devices [101].

In addition to these technical considerations, the requirements of the market must be taken into account as well; this determines a constant demand of devices characterized by low cost and power consumption, small size, light weight, wide tunability and high performances. These motivations make the design of reconfigurable filters a particularly challenging task, under a constant attention by researchers.

The generic structure of a reconfigurable filter includes a resonator, made by various types of transmission lines, lumped elements, cavities or dielectric solids, whose resonant frequency, bandwidth or filtering nature is modified by tuning elements [102].

From the point of view of classification, these devices can be categorized on the basis of their resonators. Bearing this in mind, the three main categories consist in 3D, planar, or lumped LC structures. The first one includes resonators made by waveguides (e.g. substrate integrated waveguides - SIW), cavities (e.g. evanescent-mode resonators - EVA) and dielectric resonators (DR). For the sake of brevity, resonators exploiting acoustic or ferromagnetic principles are not discussed in the present treatise. The second category is composed by resonant structures made with CPW, microstrip and striplines, generally arranged according to different layouts, such as comb-line, Hairpin or edge-coupled configurations. LC structures are usually employed at lower frequencies (<1 GHz), as the wavelength of signals would make inconvenient the use of planar structures [103].

The reconfigurability of these devices is provided by tuning elements, which are generally represented by banks of capacitors, varactors, switches to select reactive loads, or actuation mechanisms that modify the dimensional (and thus electrical) features of the resonator.

RF-MEMS technology applied as a valuable candidate for widening reconfigurability in filters since the early 2000s [104], capitalizing on its intrinsic high quality factor (Q), negligible losses and power consumption, and simple biasing of its switches and lumped components. For the sake of completeness, semiconductors represent another common choice as tuning element, but they are employed only when a short switching time is a primary concern, due to their inconvenient losses and quality factor [105]. Filters can be evaluated on the basis of power handling and consumption, linearity and tuning speed, but features like Q, tuning range, Insertion and Return Loss, size and integrability with common electronic supports, remain the most accepted figures of merit.

Considering the vast amount of literature in this field, some interesting research solutions of the last half decade are reported in the next paragraphs. Tables 7 and 8 are provided along the present section, for a better comparison of the different research items in terms of their features.

6.1. Three-dimensional

Regarding resonators based on waveguides, K band application and a high Q factor are the target of the bandpass filters reported in [106]. Among the different discussed realizations, an interesting realization is the one adopting virtual movable walls. In this approach, the resonator is obtained by inserting spaced metallic septa along the E-plane (the plane along which electric field propagates) in the center of the waveguide. The lateral walls of the waveguide facing the septa present a recess, and six dies are arranged on the wall. Each die is composed by a quartz substrate on which a conductive path can be allowed or avoided by an ohmic switch. The actuation of the switches allows to establish a conductive path that will electrically "hide" the lateral recess of the guide, varying the electrical effective width of the resonant cavity represented by the space between the central septa and lateral walls. This configuration allowed a 725 MHz shift from the basic resonant frequency (22.17 GHz). Although its Q factor and electrical performances are remarkable, the device is characterized by the typically huge dimensions and aspect ratio of waveguide-based devices. In fact, the overall length (48 mm) makes this device more suitable for fixed infrastructures.

Another bandpass implementation featuring waveguide resonant cavities is provided by [107], in which an alternation of inverters and cavities composes the whole structure. The three stages of inverters consist in dielectric substrate laminates on which RF-MEMS switches are integrated, whose activation allows a 2,4 GHz tuning range for the resonance of the two cavities, up to 14.6 GHz, by three possible intermediate steps. Also in the case of this device for Ku band applications, a remarkable Q factor is achieved for the three states, at the expenses of volume and aspect ratio.

Regarding resonators based on EVA cavities, K and Ka are the bands selected by the Authors of [108][109], for their bandpass filter. The structure of the resonator is traditional: a gold-sputtered cavity on silicon substrate, encompassing two posts, and covered by a diaphragm. The two areas of the diaphragm near the posts are provided with electrodes, for a variable deflection of the two areas toward the underlying posts. In this configuration, the resonant frequency (20 GHz) of the cavity can be shifted through the deflection, which modifies the capacitance between the posts and the corresponding areas of the diaphragm. This architecture enabled a high Q factor and an outstanding continuous tuning range of 20 GHz, still maintaining good electrical performances. The price to pay for such achievements corresponds to the typical drawbacks of micromachined 3D resonators: increased complexity of fabrication and large actuation voltages.

The same arrangement is adopted for the development of the tunable filter presented in [110], operating in V band. The two-pole filter demonstrated a fairly wide tuning range ((57.7-63) GHz) and limited Insertion Loss, featuring a CPW-microstrip transition for a simpler integration on planar layout technologies. The integration is simplified also by virtue of a further advance in the miniaturization of such device, whose size does not exceed 5x8 mm_2.

A similar arrangement is proposed for Ku band operations in [111], with a copper cavity encompassing two internal posts and fed by CPW line. In this case two implementations are offered, one using clamped-clamped RF-MEMS structures, and the other using disk-shaped patches of Vanadium Dioxide (VO_2) as tuning mechanism controlling the areas of the diaphragm facing the posts. The second approach involves a thermal activation of such material to trigger an abrupt change of conductivity (metal-to-insulator transition) of the material, determining in turn a variation of the parasitic capacitance between the disks and the upper part of the posts. This strategy allowed to achieve 1 GHz tuning range from the original resonant frequency (14.7 GHz), still providing a satisfying Q factor and reasonable electrical performances.

Table 7 Comparison between the different discussed realizations of filters. Reported values of Return Loss and Insertion Loss refer to the worst assumed value.

Work	Type (BP/BS)	Tuning Range (%)	Q unloaded	Ret. Loss (dB)	Ins. Loss (dB)	Actuation (V)
[106]	BP	3.2	1450	-13	-1.3	70
[107]	BP	18	1700	-15	-0.7	100
[108]	BP	100	540	-15	-3.09	180
[110]	BP	9	330	-	-2.9	140
[111]	BP	7	1198	-14	-2.26	-
[112]	BP	200	64	-10.5	-3.5	0.5
[113]	BP	3	3850	-	-0.44	-
[114]	BP	35	92	-10	-4.29	-
[115]	BP	19	22	-15	-0.2	

Another analog filter based on metallic cavity and inner post is provided by [112]. This implementation involves a sort of inverted arrangement: the post arises in the vertical direction from the upper side, facing the movable membrane on the bottom side of the cavity. Among the different realizations, the most interesting one is represented by a 45° top-angled post facing the gold plate tuned by thermally driven actuators. The need for a precise and constant control over the position of the membrane determines the presence of a sensing capacitance and a polysilicon thermometer under the membrane, enabling a closed-loop control of the power supplied to the actuators. The simulated performances of such arrangement demonstrated a wide continuous tuning range, concerning C, X, and Ku bands in the (6-18) GHz interval and limited Insertion Loss. In addition, the device requires less than 0.5 V for a remarkably fast actuation (1 μs).

A more traditional filter based on cavity and posts is described in [113], whose tuning principle is utilized in commercial Omron MEMS switches; switches may establish or avoid the connection to ground for a couple of striplines inserted in the cavity, fed by common SubMiniature-version-A (SMA) probes. The absence of lumped components allowed the Authors to avoid undesired degradation of the high Q factor for this 2-bit device, greater than 2000 for all the tuning states. Designed for C band applications, the filter demonstrated minimal Insertion Loss (<-0.44 dB) within a relatively limited 530 MHz tuning range in the vicinity of the designed frequency of 7 GHz.

Regarding resonators based on SIW, [114] proposes a couple of realizations, employing folded-ridged quarter-mode SIW resonators, and operating at L and S bands. In both the bandpass realizations, the tuning mechanism comprises a couple of commercial SP4T RF-MEMS switches, selecting lumped reactive loads, while the two-pole resonator is represented by two folded-ridged SIW cavities coupled by a iris opening. A quarter-mode resonator SIW is obtained by cutting a SIW waveguide along a plane of symmetry of the resonance associated with its fundamental mode. This strategy enabled a substantial miniaturization of a single SIW-based resonator, featuring a $\lambda/16$ transverse width as compared to the reported state of the art regarding such devices. In terms of electrical performance, the filter equipped with capacitive loads exhibits reasonable Insertion and Return Loss along its eight tuning states, providing a 305 MHz tuning range in the vicinity of the center operational frequency (865 MHz).

Another interesting implementation is described in [115], involving a half-mode SIW resonator loaded by a complementary split ring resonator (CSRR) and a MEMS movable membrane. In this arrangement, the CSRR in engraved on top of the 6x6 mm_2 half mode SIW, and an overhead metallic movable membrane realizes the tuning, acting as variable capacitance. This configuration determined a satisfying 500 MHz tuning range, starting from the basic resonant frequency (3.15 GHz). In addition, simulations show a remarkably small Insertion Loss (<-0.2 dB) and appreciable Return Loss (>-15 dB) for the reported tuning states.

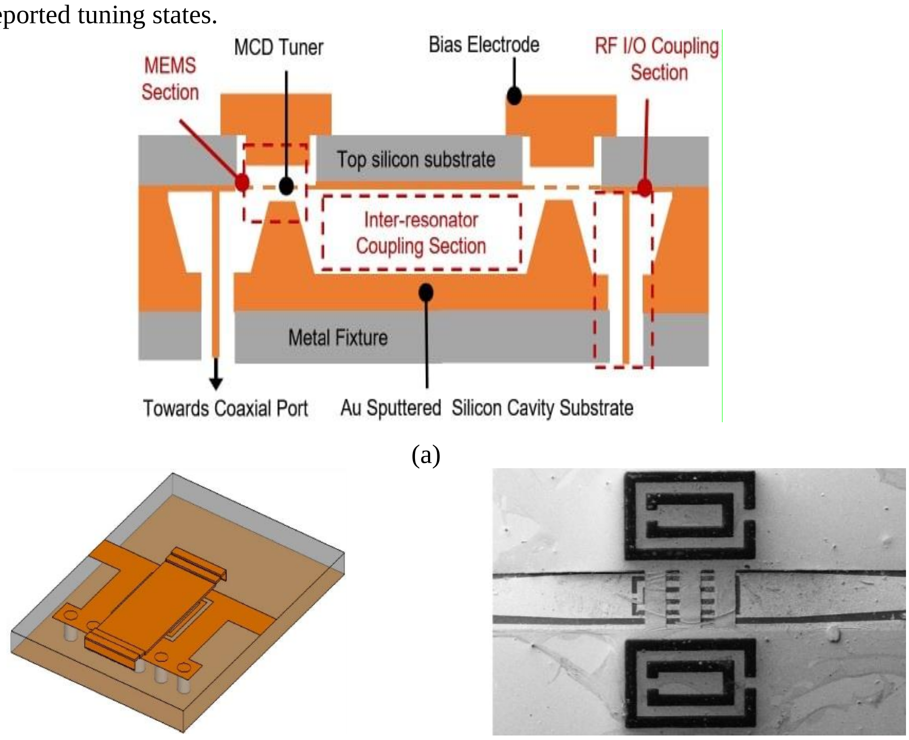

(a)

(b) (c)

Fig. 9 (a) Explanatory cross section of the EVA cavities described in [108] and [109], (b) 3D model of the device reported in [115], (c) Scanning Electron Microscope (SEM) photography of the layout realized in [116].

6.2. Planar Structures

Regarding filters based on planar structures, the first proposed device [116] is a tunable bandstop filter for Ka-band applications, realized in CPW configuration. The resonance is achieved by arranging a CSRR both on the signal line and ground sides. The default resonance frequency (38.8 GHz) can be shifted to 35.32 GHz by the activation of three movable membranes on top of the resonator engraved on the signal line, letting them act as varactors. The novelty of this research contribution is represented by the fact of being the first proposal for CPW filter based on CSRR, compatible with CMOS technology. The device, featuring a gold metallization on a silicon substrate is remarkable also in terms of dimensions, not exceeding 1.46x5 mm_2.

The same frequency band is targeted in [117], in which a bandstop filter based on shape defected ground (SDG) is presented. More specifically, the device consists in a CPW configuration, periodically loaded by four recesses with spiral-shaped metal engravings, on both its ground planes. The resonant frequency (26 GHz) of this arrangement is controlled by a SPST RF- MEMS switch on each spiral, whose actuation increases the overall length of the spiral itself. The reported simulations show an encouraging 3 GHz tuning range and a remarkable stopband attenuation.

An interesting contribution comes from [118], combining Spurline and DMTL approaches to obtain a tunable bandstop filter working at Ku band. In Spurline-based filters, the resonance is achieved by short-ended stubs along the signal line of a CPW. In this case, reconfigurability is enforced by shunt capacitive MEMS switches, whose actuation determines a reduced length of the stubs and thus a shift in the resonant frequency (18 GHz). The whole 1.2x10 mm_2 device is composed by three sections: two sections, each one loaded by a couple of stubs, and an interposed section. In the latter, the signal line is periodically equipped with three overhead movable MEMS membrane, realizing a typical DMTL configuration. The actuation of such membranes is intended in order to tune the bandwidth of the filter, thus realizing a reconfigurable device both in terms of frequency and bandwidth. From a quantitative point of view, the filter shows good performance within its 2.5 GHz tuning range; the filter also provides minimal Insertion Loss (<-1 dB) while non-operational, and remarkably large attenuation level (>-70 dB) for all its tuning states. A similar approach is adopted in [119], with two cascaded sections of CPW loaded in DMTL fashion, coupled by series capacitive RF-MEMS switches.

Targeting C band and high attenuation along the stopband, [120] proposes a three-pole bandpass filter encompassing commercial components. In fact, the three cascaded half-wavelength resonators are realized by microstrip on Roger RO4003C substrate, while each digital variable capacitor loading a resonator is a commercial product by Cavendish Kinetics. The resulting device is quite compact, providing a wide tuning range by means of 5 states covering the (5.3-7) GHz interval. In each state, the attenuation along the stopband is greater than -30 dB up to 10 GHz, still maintaining limited losses. A comparable architecture for L band applications is described in [121], comprising a three-pole resonator made by coupled quarter-wavelength sections of microstrip in combline configuration. Commercial RF-MEMS varactors are employed for tuning the basic resonant frequency (2.1 GHz) and for the control over the capacitive coupling between the two microstrip resonators. Also in this case, the layout is quite compact, since the size does not exceed 9x5 mm_2; the attenuation in the stopband is comparable as well. With the proposed device, a remarkable 700 MHz tuning range can be achieved by 21 capacitance states, with appreciable electrical performances.

Table 8 Comparison between the different discussed realizations of filters. Reported values of Return Loss and Insertion Loss refer to the worst assumed value.

Work	Type (BP/BS)	Tuning Range (%)	Q unloaded	Ret. Loss (dB)	Ins. Loss (dB)	Actuation (V)
[116]	BS	10	-	-2	-31	25.65
[117]	BS	10	-	-3	-42	-
[118]	BS	16	-	-10	-75	-
[120]	BP	32	200	-17.5	-5.3	-
[121]	BP	50	253	-20	-2	30
[122]	BP	650	-	-12.7	-6.8	40

A tunable bandpass filter covering almost the entire UHF band is presented in [122]. The basic structure is represented by a half-wavelength and a quarter-wavelength microstrip resonator in concentric/nested arrangement. A couple of RF-MEMS switches control the activation of each resonator, so that the activation of one, of the other, or of both resonators, realizes a first coarse tuning of the resonant frequency. The fine tuning is then performed by a bank of switched capacitors connected to each resonator. The choice of the nested arrangement allowed the Authors to achieve fairly limited dimensions (26x36 mm_2), for a device working at relatively low frequencies, fabricated on common RT/Duroid substrate and equipped with commercial lumped components. In terms of capabilities, the wide tuning range ((0.4-3) GHz) of such device is inevitably counterbalanced by contained electrical performances.

7. Conclusions

The abovementioned examples of RF-MEMS devices portray the current state of the art of a technology that is now mature to face current challenges posed by the 5G applications. Besides the intrinsic reconfigurability, considerable wideband performances and low power consumption, research on RF MEMS has provided components characterized by an increasing miniaturization and reliability, manageable control signals, and compatibility with existing technologies. Among the different proposals, while some may seem more appropriate for fixed infrastructures, other may apply to mobile low power devices for their limited size and control voltage. Many devices proved a satisfying reliability under extensive power and temperature measurements, reinforced by low cost and effective packaging strategies. The range of frequencies covered by the mentioned examples comprehend both portions below 6 GHz and higher ones, involving all those bands engaged in the realization of 5G infrastructure. In addition to the previous considerations, the electrical performances of the reported RF MEMS devices proved themselves to be a valuable plus of this technology, in view of a potentially significant role in 5G scenario.

Acknowledgement: *This paper is published thanks to the support of the project "Wafer Level Micropackaging di RF MEMS switch per applicazioni spaziali" (F36C18000400005) funded by the Agenzia Spaziale Italiana (ASI).*

REFERENCES

[1] G. Tagliapietra and J. Iannacci, "Overview of recent developments in rf-mems technology with reference to 5g emerging applications," In Proceedings of the 1st International Conference on Micro/Nanoelectronics Devices, Circuits and Systems (MNDCS 2021), pages 1–31, 2021.

[2] J. Iannacci, "Rf-mems: an enabling technology for modern wireless systems bearing a market potential still not fully displayed," *Microsystem Technologies*, vol. 14, no. 09, 2015.

[3] Omron Website. Omron electronic components. [online], Accessed: Nov. 19, 2020. https://www.components.omron.com/.

[4] L. Wood, "Global radio frequency (rf) mems market 2019-2023: Expected to grow at a cagr of approx 37%, with aac technologies, analog devices, broadcom, cavendish kinetics, and qorvo at the forefront-researchandmarkets.com", [online], Accessed: 19 November 2020, https://www.businesswire.com/news/home/20190221005400/en/Global-Radio-Frequency-RF-MEMS-Market-2019-2023/ .

[5] Cavendish Kinetics, "Cavendish powers nubia z9: world's first smartphone with dual antenna tuning," [online], Accessed: 19 November 2020. https://www.cavendish-kinetics.com/release/cavendish-powers-nubia-z9-worlds-first-smartphone-with-dual-antenna-tuning/ .

[6] J. Iannacci, "Internet of things (iot); internet of everything (ioe); tactile internet; 5g - a (not so evanescent) unifying vision empowered by eh-mems (energy harvesting mems) and rf-mems (radio frequency mems)," *Sensors and Actuators A: Physical*, vol. 272, no. 02, 2018.

[7] J. Rodriguez. Fundamentals of 5G Mobile Networks. Wiley, 2015.

[8] GSM Association. 5g spectrum - public policy position. [online], Accessed: 19 November 2020. https://www.gsma.com/spectrum/wp-content/uploads/2020/03/5G-Spectrum-Positions.pdf .

[9] J. Iannacci, "Rf-mems technology: An enabling solution in the transition from 4g-lte to 5g mobile applications," In 2017 IEEE SENSORS, 2017, pp. 1–3.

[10] J. Iannacci, "Rf-mems for high-performance and widely reconfigurable passive components - a review with focus on future telecommunications, internet of things (iot) and 5g applications", *Journal of King Saud University - Science*, vol. 29, no. 4, pp. 436–443, 2017. SI: Smart materials and applications of new materials.

[11] L. Ma, N. Soin, M. H. Mohd Daut, and S. F. Wan Muhamad Hatta, "Comprehensive study on rf-mems switches used for 5g scenario", *IEEE Access*, vol. 7, pp. 107506-107522, 2019.

[12] Y. Yuan-Wei, Z. Jian, J. Shi-Xing, and Y. Shi, "A high isolation series-shunt rf mems switch", *Sensors*, vol. 9, no. 6, pp. 4455–4464, 2009.

[13] J. Sun, Z. Li, J, Zhu, Y. Yu, and L. Jiang, "Design of dc-contact rf mems switch with temperature stability", *AIP Advances*, vol. 5, March 2015.

[14] S. T. Wipf, A. Goritz, M. Wietstruck, C. Wipf, B. Tillack, and M. Kaynak, "D-band rf-mems spdt switch in a 0.13 um sige bicmos technology", *IEEE Microwave and Wireless Components Letters*, vol. 26, pp. 1002–1004, 2016.

[15] Y. Liu, Y. Bey, and X. Liu, "High-power high-isolation rf-mems switches with enhanced hotswitching reliability using a shunt protection technique", *IEEE Transactions on Microwave Theory and Techniques*, vol. 65, no. 9, pp. 3188–3199, 2017.

[16] C. Chu and X. Liao, "One to 40ghz ultra-wideband rf mems direct-contact switch based on gaas mmic technique", *IET Microwaves, Antennas Propagation*, vol. 12, no. 6pp. 879–884, 2018.

[17] S. Dey, S. Koul, A. Poddar, and U. Rohde, "Compact, broadband and reliable lateral mems switching networks for 5g communications", *Progress in Electromagnetics Research M*, vol. 86 pp. 163–171, 2019.

[18] N. Narang and P. Singh, "Metal contact rf mems switch design for high performance in ka band", In Proceedings of the IOP Conference Series: Materials Science and Engineering, vol. 872, p. 012020, 06 2020.

[19] H. Yang, H. Zareie, and G. M. Rebeiz, "A high power stress-gradient resilient rf mems capacitive switch", *Journal of Microelectromechanical Systems*, vol. 24, no. 3, pp. 599–607, 2015.

[20] K. Demirel, E. Yazgan, S. Demir, and T. Akin, "A folded leg ka-band rf mems shunt switch with amorphous silicon (a-si) sacrificial layer", *Microsystem Technologies*, vol. 23, pp. 1191–1200, 2017.

[21] M. Li, J. Zhao, Z. You, and G. Zhao, "Design and fabrication of a low insertion loss capacitive rf mems switch with novel micro-structures for actuation", *Solid-State Electronics*, vol. 127, pp. 32–37, 2017.

[22] G. S. Kondaveeti, K. Guha, S. R. Karumuri, and A. Elsinawi, "Design of a novel structure capacitive rf mems switch to improve performance parameters", *IET Circuits, Devices Systems*, vol. 13, no. 7, pp. 1093–1101, 2019.

[23] U. Chae, H. Y. Yu, C. Lee, and I. J. Cho, "A hybrid rf mems switch actuated by the combination of bidirectional thermal actuations and electrostatic holding", *IEEE Transactions on Microwave Theory and Techniques*, vol. 68, no. 8, pp. 3461–3470, 2020.

[24] A. Bojesomo, N. Saeed, and I. M. Elfadel, "A multiband rf mems switch with low insertion loss and cmos-compatible pull-in voltage" In Proceedings of the 2018 Symposium on Design, Test, Integration Packaging of MEMS and MOEMS (DTIP), 2018, pp. 1–4.
[25] W. Tian, P. Li, and L.X. Yuan, "Research and analysis of mems switches in different frequency bands", *Micromachines*, vol. 9, no. 04, 2018.
[26] A. Algamili, M. Haris, Md Khir, J. Dennis, A. Ahmed, S. Omar, S. Ba Hashwan, and M. Junaid, "A review of actuation and sensing mechanisms in mems-based sensor devices", *Nanoscale Research Letters*, 01 2021.
[27] D. A. Czaplewski, C. W. Dyck, H. Sumali, J. E. Massad, J. D. Kuppers, I. Reines, W. D. Cowan, and C. P. Tigges, "A soft-landing waveform for actuation of a single-pole single-throw ohmic rf mems switch", *Journal of Microelectromechanical Systems*, vol. 15, no. 6, pp. 1586–1594, 2006.
[28] D. Peroulis, S. P. Pacheco, K. Sarabandi, and L. P. B. Katehi, "Electromechanical considerations in developing low-voltage rf mems switches", *IEEE Transactions on Microwave Theory and Techniques*, vol. 51, no. 1, pp. 259–270, 2003.
[29] S. Fouladi and R. R. Mansour, "Capacitive rf mems switches fabricated in standard 0.35-um cmos technology", *IEEE Transactions on Microwave Theory and Techniques*, vol. 58, no. 2, pp. 478–486, 2010.
[30] A. Gopalan and U. K. Kommuri, "Design and development of miniaturized low voltage triangular rf mems switch for phased array application", *Applied Surface Science*, vol. 449, pp. 340–345, 2018. 4th International Conference on Nanoscience and Nanotechnology.
[31] H. Wei, Z. Deng, X. Guo, Y. Wang, and H. Yang, "High on/off capacitance ratio RF MEMS capacitive switches", *Journal of Micromechanics and Microengineering*, vol. 7, no. 5, p. 055002, Mar 2017.
[32] J. Iannacci, A. Repchankova, D. Macii, and M. Niessner, "A measurement procedure of technology-related model parameters for enhanced rf-mems design", In Proceedings of the 2009 IEEE International Workshop on Advanced Methods for Uncertainty Estimation in Measurement, pp. 44–49, 2009.
[33] J. Iannacci, "Mixed-Domain Fast Simulation of RF and Microwave MEMS-based Complex Networks within Standard IC Development Frameworks", 04, 2010.
[34] J.-M. Kim, J.-H. Park, C.-W. Baek, and Y.-K. Kim, "The siog-based single-crystalline silicon (scs) rf mems switch with uniform characteristics", *Journal of Microelectromechanical Systems*, vol. 13, no. 6, pp. 1036–1042, 2004.
[35] A. Persano, A. Tazzoli, P. Farinelli, G. Meneghesso, P. Siciliano, and F. Quaranta, "K-band capacitive mems switches on gaas substrate: Design, fabrication, and reliability", *Microelectronics Reliability*, vol. 52, no. 9, pp. 2245–2249, 2012.
[36] S. Touati, N. Lorphelin, A. Kanciurzewski, R. Robin, A. Rollier, O. Millet, and K. Segueni, "Low actuation voltage totally free flexible rf mems switch with antistiction system", In Proceedings of the 2008 Symposium on Design, Test, Integration and Packaging of MEMS/MOEMS, 2008, pp. 66–70.
[37] J. Y. Park, G. H. Kim, K. W. Chung, and J. U. Bu, "Fully integrated micromachined capacitive switches for rf applications", In Proceedings of the 2000 IEEE MTT-S International Microwave Symposium Digest (Cat. No.00CH37017), vol. 1, pp. 283–286, 2000.
[38] A. Persano, A. Cola, G. De Angelis, A. Taurino, P. Siciliano, and F. Quaranta. "Capacitive rf mems switches with tantalum-based materials", *Journal of Microelectromechanical Systems*, vol. 20, no. 2, pp. 365–370, 2011.
[39] M. Angira, G.M. Sundram, K. Rangra, D. Bansal, and K. Maninder, "On the investigation of an interdigitated, high capacitance ratio shunt rf-mems switch for x- band applications", 05, 2013.
[40] V. Mulloni, F. Solazzi, G. Resta, F. Giacomozzi, and B. Margesin, "Rf-mems switch design optimization for long-term reliability" In Proceedings of the 2013 Symposium on Design, Test, Integration and Packaging of MEMS/MOEMS (DTIP), 2013, pp. 1–6.
[41] P. Blondy, A. Crunteanu, C. Champeaux, A. Catherinot, P. Tristant, O. Vendier, J. L. Cazaux, and L. Marchand, "Dielectric less capacitive mems switches", In Proceedings of the 2004 IEEE MTT-S International Microwave Symposium Digest (IEEE Cat. No.04CH37535), vol 2, pp. 573–576, 2004.
[42] F. Ke, J. Miao, and J. Oberhammer, "A ruthenium-based multimetal-contact rf mems switch with a corrugated diaphragm", *Journal of Microelectromechanical Systems*, vol. 17, no. 6, pp. 1447–1459, 2008.
[43] C. D. Patel and G. M. Rebeiz, "A high-reliability high-linearity high-power rf mems metal-contact switch for dc-40-ghz applications" *IEEE Transactions on Microwave Theory and Techniques*, vol. 60, no. 10, pp. 3096–3112, 2012.
[44] J. Pal, Y. Zhu, J. Lu, D. Dao, and F. Khan, "High power and reliable spst/sp3t rf mems switches for wireless applications" *IEEE Electron Device Letters*, vol. 37, no. 9, pp. 1219–1222, 2016.
[45] M. Fernandez-Bolanos Badia, E. Buitrago, and A. M. Ionescu, "Rf mems shunt capacitive switches using aln compared to Si3N4 dielectric", *Journal of Microelectromechanical Systems*, vol. 21, no. 5, pp. 1229–1240, 2012.

[46] C. Harendt, H. Graf, B. Hofflinger, and E. Penteker, "Silicon fusion bonding and its characterization", *Journal of Micromechanics and Microengineering*, vol. 2, no. 113, 01, 1999.
[47] W. Tian, X. Wang, J. Niu, H. Cui, Y. Chen, and Y. Zhang, "Research status of wafer level packaging for rf mems switches" In Proceedings of the 21st International Conference on Electronic Packaging Technology (ICEPT)", 2020, pp. 1–5.
[48] F. Giacomozzi, V. Mulloni, S. Colpo, A. Faes, G. Sordo, and S. Girardi, "Rf-mems devices packaging by using quartz caps and epoxy polymer sealing rings", In Proceedings of the 2013 Symposium on Design, Test, Integration and Packaging of MEMS/MOEMS (DTIP), 2013, pp 1–6.
[49] T. Katsuki, T. Nakatani, H. Okuda, O. Toyoda, S. Ueda, and F. Nakazawa, "A highly reliable single-crystal silicon rf-mems switch using au sub-micron particles for wafer level ltcc cap packaging", In Proceedings of the 2nd IEEE CPMT Symposium Japan, 2012, pp. 1–4.
[50] S. Seok, J. Kim, M. Fryziel, N. Rolland, P. Rolland, H. Maher, W. Simon, and R. Baggen, "Wafer-level bcb cap packaging of integrated mems switches with mmic", In Proceedings of the IEEE/MTT-S International Microwave Symposium Digest, 2012, pp. 1–3.
[51] R. Goggin, P. Fitzgerald, B. Stenson, E. Carty, and P. McDaid, "Commercialization of a reliable rf mems switch with integrated driver circuitry in a miniature qfn package for rf instrumentation applications" In Proceedings of the IEEE MTT-S International Microwave Symposium, 2015, pp. 1–4.
[52] I. Comart, C. Cetintepe, E. Sagiroglu, S. Demir, and T. Akin, "Development and modeling of a wafer-level bcb packaging method for capacitive rf mems switches", *Journal of Microelectromechanical Systems*, vol. 28, no. 4, pp. 724–731, 2019.
[53] F. Barriere, A. Crunteanu, A. Bessaudou, A. Pothier, F. Cosset, D. Mardivirin, and P. Blondy. Zero level metal thin film package for rf mems. In 2010 Topical Meeting on Silicon Monolithic Integrated Circuits in RF Systems (SiRF), pages 148-151, 2010.
[54] K. Nadaud, F. Roubeau, A. Pothier, P. Blondy, L. Zhang, and R. Stefanini, "High q zero level packaged rf-mems switched capacitor arrays", In Proceedings of the 11th European Microwave Integrated Circuits Conference (EuMIC), 2016, pp. 448–451.
[55] F. Souchon, D. Saint-Patrice, J. L. Pornin, D. Bouchu, C. Baret, and B. Reig, "Thin film packaged redundancy rf mems switches for space applications, In Proceedings of the 19th International Conference on Solid-State Sensors, Actuators and Microsystems (TRANSDUCERS), 2017, pp. 175–178.
[56] S. T. Wipf, A. Goritz, M. Wietstruck, C. Wipf, B. Tillack, A. Mai, and M. Kaynak, "Thin film wafer level encapsulated rf-mems switch for d-band applications" In Proceedings of the 11th European Microwave Integrated Circuits Conference (EuMIC), 2016, pp. 452–455.
[57] N. Belkadi, K. Nadaud, C. Hallepee, D. Passerieux, and P. Blondy, Zero-level packaged rf-mems switched capacitors on glass substrates, *Journal of Microelectromechanical Systems*, vol. 29, no. 1pp. 109–116, 2020.
[58] A. Persano, F. Quaranta, A. Taurino, P. Siciliano, and J. Iannacci, "Thin film encapsulation for rf mems in 5g and modern telecommunication systems", *Sensors*, vol. 20, pp. 1–12, 04, 2020.
[59] A. Malczewski, S. Eshelman, B. Pillans, J. Ehmke, and C. L. Goldsmith, "X-band rf mems phase shifters for phased array applications", *IEEE Microwave and Guided Wave Letters*, vol. 9, no. 12, pp. 517–519, 1999.
[60] S. Barker and G. M. Rebeiz, "Distributed mems true-time delay phase shifters and wide-band switches", *IEEE Transactions on Microwave Theory and Techniques*, vol. 46, no. 11, pp. 1881–1890, 1998.
[61] A. S. Nagra and R. A. York, "Distributed analog phase shifters with low insertion loss", *IEEE Transactions on Microwave Theory and Techniques*, vol. 47, no. 9, pp. 1705–1711, 1999.
[62] S. Koul and S. Dey, "Radio Frequency Micromachined Switches, Switching Networks, and Phase Shifters", CRC Press, May 2019.
[63] Y.A. Wang, "RF MEMS Switches and Phase Shifters for 3D MMIC Phased Array Antenna Systems", University of Cincinnati, 2002.
[64] A. Chakraborty and B. Gupta, "Paradigm phase shift: Rf mems phase shifters: An overview", *IEEE Microwave Magazine*, vol. 18, no. 1, pp. 22–41, 2017.
[65] G. M. Rebeiz, Guan-Leng Tan, and J. S. Hayden, "Rf mems phase shifters: design and applications", *IEEE Microwave Magazine*, vol. 3, no. 2, pp. 72–81, 2002.
[66] J. Lampen, S. Majumder, C. Ji, and J. Maciel, "Low-loss, mems based, broadband phase shifters", In Proceedings of the IEEE International Symposium on Phased Array Systems and Technology, 2010, pp. 219–224.
[67] R. Malmqvist, C. Samuelsson, B. Carlegrim, P. Rantakari, T. Vaha-Heikkilla, A. Rydberg, and J. Varis, "Ka-band rf mems phase shifters for energy starved millimetre-wave radar sensors", In Proceedings of the CAS (International Semiconductor Conference), 2010, vol. 1, pp. 261–264.
[68] T. Watanabe, R. Yamazaki, T. Furutsuka, S. Tanaka, and K. Suzuki, "A quasi-millimeter wave band phase shifter with mems shunt switches" In Proceedings of the Asia-Pacic Microwave Conference, 2014, pp. 64–66.

[69] Y. Huang, J. Bao, X. Li, Y. Wang, and Y. Du, "A 4-bit switched-line phase shifter based on mems switches" In Proceedings of the 10th IEEE International Conference on Nano/Micro Engineered and Molecular Systems, 2015, pp. 405–408.
[70] S. Dey and S. K. Koul, "Reliability analysis of ku-band 5-bit phase shifters using mems sp4t and spdt switches", *IEEE Transactions on Microwave Theory and Techniques*, vol. 63, no. 12, pp. 3997-4012, 2015.
[71] S. Koul, S. Dey, A. Poddar, and U. Rohde, "Ka-band reliable and compact 3-bit true-time-delay phase shifter using mems single-pole-eight-throw switching networks", *Journal of Micromechanics and Microengineering*, vol. 26, 08 2016.
[72] S. K. Koul, S. Dey, A. K. Poddar, and U. L. Rohde, "Micromachined switches and phase shifters for transmit/receive module applications", In Proceedings of the 46th European Microwave Conference (EuMC), 2016, pp. 971–974.
[73] J. Iannacci, G. Resta, A. Bagolini, F. Giacomozzi, E. Bochkova, E. Savin, R. Kirtaev, A. Tsarkov, and M. Donelli, "Rf-mems monolithic k and ka band multistate phase shifters as building blocks for 5g and internet of things (iot) applications", *Sensors*, vol. 20, no. 13, 05, 2020.
[74] J. Reinke, L.Wang, G. K. Fedder, and T. Mukherjee, "A 4-bit rf mems phase shifter monolithically integrated with conventional cmos", In Proceedings of the IEEE 24th International Conference on Micro ElectroMechanical Systems, 2011, pp. 748–751.
[75] Y. Lin, Y. Chou, and C. Chang, "A balanced digital phase shifter by a novel switching-mode topology", *IEEE Transactions on Microwave Theory and Techniques*, vol. 61, no. 6, 2361–2370, 2013.
[76] M. Bakri-Kassem and R. R. Mansour, "A novel self collapsed corrugated mems phase shifter", In Proceedings of the 2013 European Microwave Integrated Circuit Conference, 2013, pp. 360–363.
[77] A. Razeghi and B. A. Ganji, "An improved switched-line phase shifter using distributed mems transmission line", *Majlesi Journal of Telecommunication Devices*, vol. 4, no. 3, Nov. 2015.
[78] A. Chakraborty and B. Gupta, "Utility of rf mems miniature switched capacitors in phase shifting applications", *AEU - International Journal of Electronics and Communications*, vol. 75, 03 2017.
[79] S. Afrang, K. Samandari, and G. Rezazadeh, "A small size ka band six-bit dmtl phase shifter using new design of mems switch", *Microsystem Technologies*, vol. 23, 06 2017.
[80] S. Dey and S. Koul, "Design, development and characterization of an x-band 5 bit dmtl phase shifter using an inline mems bridge and mam capacitors", *Journal of Micromechanics and Microengineering*, vol. 24, 09 2014.
[81] S. Dey and S. Koul, "10-25 ghz frequency reconfigurable mems 5-bit phase shifter using push-pull actuator based toggle mechanism", *Journal of Micromechanics and Microengineering*, vol. 25, 2015.
[82] S. Dey, S. Koul, A. Poddar, and U. Rohde, "Ku to v-band 4-bit mems phase shifter bank using high isolation sp4t switches and dmtl structures", *Journal of Micromechanics and Microengineering*, vol. 27, p. 105010, 2017.
[83] A. S. Abdellatif, M. Faraji-Dana, N. Ranjkesh, A. Taeb, M. Fahimnia, S. Gigoyan, and S. Safavi- Naeini, "Low loss, wideband, and compact cpw-based phase shifter for millimeter-wave applications", *IEEE Transactions on Microwave Theory and Techniques*, vol. 62, no. 12, pp. 3403–3413, 2014.
[84] S. Dey, S. K. Koul, A. K. Poddar, and U. L. Rohde, "Reliable and compact 3- and 4-bit phase shifters using mems sp4t and sp8t switches", *Journal of Microelectromechanical Systems*, vol. 27, no. 1, pp. 113–124, 2018.
[85] W. Tian, Y. Zhang, M. Li, Z. Xie, and W. Li, "5-bit spiral distributed rf mems phase shifter. In 2019 IEEE 19th International Conference on Nanotechnology (IEEE-NANO)", 2019, pp. 94–98.
[86] B. Belenger, B. Espana, S. Courreges, P. Blondy, O. Vendier, D. Langrez, and J. Cazaux, "A high-power ka-band rf-mems 2-bit phase shifter on sapphire substrate", In Proceedings of the 6th European Microwave Integrated Circuit Conference, 2011, pp 164–167.
[87] B. Pillans, L. Coryell, A. Malczewski, C. Moody, F. Morris, and A. Brown, "Advances in rf mems phase shifters from 15 ghz to 35 ghz", In Proceedings of the IEEE/MTT-S International Microwave Symposium Digest, 2012, pp. 1–3.
[88] C. Ko, K. M. J. Ho, and G. M. Rebeiz, "An electronically-scanned 1.8-2.1 ghz base-station antenna using packaged high-reliability rf mems phase shifters", *IEEE Transactions on Microwave Theory and Techniques*, vol. 61, no. 2, pp. 979–985, 2013.
[89] X. Li, K. Y. Chan, and R. Ramer, "E-band rf mems differential reflection-type phase shifter", *IEEE Transactions on Microwave Theory and Techniques*, vol. 67, no. 12, pp. 4700–4713, 2019.
[90] O. D. Gurbuz and G. M. Rebeiz, "A 1.6{2.3-ghz rf mems reconfigurable quadrature coupler and its application to a 360 reflective-type phase shifter", *IEEE Transactions on Microwave Theory and Techniques*, vol. 63, no. 2, pp. 414–421, 2015.
[91] P. K. Shrivastava, S. K. Koul, and M. P. Abegaonkar, "Compact k-band lange coupler based 2-bit rf mems reflection-type phase shifter", In Proceedings of the 2018 IEEE MTT-S International Microwave and RF Conference (IMaRC), 2018, pp. 1–4.

[92] T. Singh, N. K. Khaira, and R. R. Mansour, “Thermally actuated soi rf mems-based fully integrated passive reflective-type analog phase shifter for mmwave applications”, *IEEE Transactions on Microwave Theory and Techniques*, pp. 1–4, 2020.

[93] J. Iannacci, F. Giacomozzi, S. Colpo, B. Margesin, and M. Bartek, “A general purpose reconfigurable mems-based attenuator for radio frequency and microwave applications”, In Proceedings of the IEEE EUROCON 2009, 2009, pp. 1197–1205.

[94] J. Iannacci, A. Faes, F. Mastri, D. Masotti, and V. Rizzoli, “A mems-based wideband multi-state power attenuator for radio frequency and microwave applications”, In Proceedings of the TechConnect World, NSTI Nanotech 2010, vol. 2, pp. 328–331.

[95] X. Guo, Z. Gong, Q. Zhong, X. Liang, and Z. Liu, “A miniaturized reconfigurable broadband attenuator based on rf mems switches”, *Journal of Micromechanics and Microengineering*, vol. 26, p. 074002, 2016.

[96] J. Sun, J. Zhu, L. Jiang, Y. Yu, and Z. Li, “A broadband dc to 20 ghz 3-bit mems digital attenuator”, *Journal of Micromechanics and Microengineering*, vol. 26, p. 055005, 05 2016.

[97] J. Iannacci, M. Huhn, C. Tschoban, and H. Potter, “Rf-mems technology for future mobile and high-frequency applications: Reconfigurable 8-bit power attenuator tested up to 110 ghz”, *IEEE Electron Device Letters*, vol. 37, no. 12, pp. 1646–1649, 2016.

[98] A. Raeesi, H. Al-Saedi, A. Palizban, A. Taeb, W. M. Abdel-Wahab, S. Gigoyan, and S. Safavi-Naeini, “Low-cost planar rf mems-based attenuator”, In Proceedings of the IEEE MTT-S International Microwave Symposium (IMS), 2019, pp. 869–872.

[99] N. K. Khaira, T. Singh, and R. R. Mansour, “Rf mems based 60 ghz variable attenuator”, In Proceedings of the IEEE MTT-S International Microwave Workshop Series on Advanced Materials and Processes for RF and THz Applications (IMWS-AMP), 2018, pp. 1–3.

[100] X. Liu, “Tunable rf and microwave filters”, In Proceedings of the IEEE 16th Annual Wireless and Microwave Technology Conference (WAMICON), 2018, pp 1–5.

[101] A. Jaimes-Vera, I. Llamas-Garro, A. Corona-Chavez, and I. Zaldivar-Huerta, “Review on microwave and millimeter filters using mems technology”, In Proceedings of the 17th International Conference on Electronics, Communications and Computers (CONIELECOMP'07), 2007, pp. 26–30.

[102] K. Thialagavthi and M. Balakumar, “Review on rf tunable filters”, *International Journal of Innovations in Engineering and technology (IJIET)*, 04 2017.

[103] F. Lin and M. Rais-Zadeh, “Tunable RF MEMS Filters: A Review”, *Encyclopedia of Nanotechnology*, pp. 4233–4243, 01 2016.

[104] J. Brank, J. Yao, M. Eberly, A. Malczewski, K. Varian, and C. Goldsmith, “Rf mems-based tunable filters”, *International Journal of RF and Microwave Computer-Aided Engineering*, vol. 11, no. 5, pp. 276–284, 2001.

[105] Z. Brito-Brito, J. Reyes, and I. Llamas-Garro, “Recent advances in reconfigurable microwave filters”, SBMO/IEEE MTT-S International Microwave and Optoelectronics Conference Proceedings, 10 2011.

[106] L. Pelliccia, F. Cacciamani, P. Farinelli, and R. Sorrentino, “High-q tunable waveguide filters using ohmic rf mems switches”, *IEEE Transactions on Microwave Theory and Techniques*, vol. 63, 10, pp. 3381–3390, 2015.

[107] L. Gong, K. Y. Chan, and R. Ramer, “A four-state iris waveguide bandpass filter with switchable irises”, 2017 IEEE MTT-S International Microwave Symposium (IMS), 2017, pp. 260–263.

[108] Z. Yang and D. Peroulis, “A 20{40 ghz tunable mems bandpass filter with enhanced stability by gold-vanadium micro-corrugated diaphragms”, In Proceedings of the IEEE MTT-S International Microwave Symposium (IMS), 2016, pp. 1–3.

[109] Z. Yang, D. Psychogiou, and D. Peroulis, “Design and optimization of tunable silicon-integrated evanescent-mode bandpass filters”, *IEEE Transactions on Microwave Theory and Techniques*, vol. 66, no. 4, pp. 1790–1803, 2018.

[110] M. Abdelfattah, D. Psychogiou, Z. Yang, and D. Peroulis, “V-band frequency reconfigurable cavity-based bandpass filters”, In Proceedings of the 2016 IEEE/ACES International Conference on Wireless Information Technology and Systems (ICWITS) and Applied Computational Electromagnetics (ACES), 2016, pp. 1–2.

[111] M. Agaty, A. Crunteanu, C. Dalmay, and P. Blondy, “Ku band high-q tunable cavity filters using mems and vanadium dioxide (vo2) tuners”, In Proceedings of the 2018 IEEE MTT-S International Microwave Workshop Series on Advanced Materials and Processes for RF and THz Applications (IMWS-AMP), 2018, pp 1–3.

[112] J. Chang, M. J. Holyoak, G. K. Kannell, M. Beacken, M. Imboden, and D. J. Bishop, “High performance, continuously tunable microwave filters using mems devices with very large, controlled, out-of-plane actuation”, *Journal of Microelectromechanical Systems*, vol. 27, no. 6, pp. 1135–1147, 2018.

[113] J. Jiang and R. R. Mansour, “High-q tunable filter with a novel tuning structure”, In Proceedings of the 11th European Microwave Integrated Circuits Conference (EuMIC), 2016, pp. 436–439, 2016.
[114] T. R. Jones and M. Daneshmand, “Miniaturized folded ridged quarter-mode substrate integrated waveguide rf mems tunable bandpass filter”, *IEEE Access*, vol. 8, pp. 115837–115847, 2020.
[115] S. Shirin Saberhosseini, B. A. Ganji, and A. Ghorbani, “Tunable and dual-band hmsiw resonator using rf mems capacitor”, In Proceedings of the Iranian Conference on Electrical Engineering (ICEE), 2017, pp 279–282.
[116] B. Pradhan and B. Gupta, “Ka-band tunable filter using metamaterials and rf mems varactors”, *Journal of Microelectromechanical Systems*, vol. 24, no. 5, pp. 1453–1461, 2015.
[117] R. Kuriakose and E. S. Shajahan, “Tunable bandstop filter based on cascaded spiral shaped defected ground plane cpw”, In Proceedings of the International Conference on Smart Electronics and Communication (ICOSEC), 2020, pp. 945–949.
[118] K. N. Jose and M. R. Baiju, “A tunable cpw spurline filter employing distributed mems switches”, In Proceedings of the IEEE Students' Technology Symposium (TechSym), 2016, pp. 235–239.
[119] R. Kumar, U. Sharma, and P. Jain, “Dmtl filter in ku-band with improved slope of attenuation after cut-off”, In Proceedings of the 5th International Conference on Signal Processing and Integrated Networks (SPIN), 2018, pp. 569–574.
[120] T. Lin, K. K. Wei Low, R. Gaddi, and G. M. Rebeiz, “High-linearity 5.3-7.0 ghz 3-pole tunable bandpass filter using commercial rf mems capacitors”, In Proceedings of the 48th European Microwave Conference (EuMC), 2018, pp. 555–558.
[121] A. J. Alazemi and G. M. Rebeiz, “A low-loss 1.4-2.1 ghz compact tunable three-pole filter with improved stopband rejection using rf-mems capacitors”, In Proceedings of the IEEE MTT-S International Microwave Symposium (IMS), 2016, pp 1–4, 2016.
[122] K. Motoi, N. Oshima, M. Kitsunezuka, and K. Kunihiro, “A band-switchable and tunable nested bandpass filter with continuous 0.4-3ghz coverage”, In Proceedings of the 46th European Microwave Conference (EuMC), 2016, pp. 1421–1424.